Modification of hERG1 channel gating by Cd^{2+}

Jennifer Abbruzzese,[1] Frank B. Sachse,[2] Martin Tristani-Firouzi,[3] and Michael C. Sanguinetti[1]

[1]Department of Physiology, [2]Department of Bioengineering, and [3]Department of Pediatrics, Nora Eccles Harrison Cardiovascular Research and Training Institute, University of Utah, Salt Lake City, UT 84112

Each of the four subunits in a voltage-gated potassium channel has a voltage sensor domain (VSD) that is formed by four transmembrane helical segments (S1–S4). In response to changes in membrane potential, intramembrane displacement of basic residues in S4 produces a gating current. As S4 moves through the membrane, its basic residues also form sequential electrostatic interactions with acidic residues in immobile regions of the S2 and S3 segments. Transition metal cations interact with these same acidic residues and modify channel gating. In human ether-á-go-go–related gene type 1 (hERG1) channels, Cd^{2+} coordinated by D456 and D460 in S2 and D509 in S3 induces a positive shift in the voltage dependence of activation of ionic currents. Here, we characterize the effects of Cd^{2+} on hERG1 gating currents in *Xenopus* oocytes using the cut-open Vaseline gap technique. Cd^{2+} shifted the half-point ($V_{1/2}$) for the voltage dependence of the OFF gating charge–voltage (Q_{OFF}-V) relationship with an EC_{50} of 171 µM; at 0.3 mM, $V_{1/2}$ was shifted by +50 mV. Cd^{2+} also induced an as of yet unrecognized small outward current ($I_{Cd\text{-}out}$) upon repolarization in a concentration- and voltage-dependent manner. We propose that Cd^{2+} and Arg residues in the S4 segment compete for interaction with acidic residues in S2 and S3 segments, and that the initial inward movement of S4 associated with membrane repolarization displaces Cd^{2+} in an outward direction to produce $I_{Cd\text{-}out}$. Co^{2+}, Zn^{2+}, and La^{3+} at concentrations that caused ∼+35-mV shifts in the Q_{OFF}-V relationship did not induce a current similar to $I_{Cd\text{-}out}$, suggesting that the binding site for these cations or their competition with basic residues in S4 differs from Cd^{2+}. New Markov models of hERG1 channels were developed that describe gating currents as a noncooperative two-phase process of the VSD and can account for changes in these currents caused by extracellular Cd^{2+}.

The Journal of General Physiology

INTRODUCTION

The human ether-á-go-go–related gene type 1 (hERG1) channel was originally cloned from a human hippocampal cDNA library (Warmke and Ganetzky, 1994) and was later reported to be highly expressed in many other cell types, where it can contribute to spike frequency adaptation, maintenance of K^+ homeostasis, set the resting membrane, or mediate action potential repolarization (Sanguinetti, 2010). hERG1 channels are also highly expressed in the heart, where they conduct the rapid delayed rectifier K^+ current, I_{Kr} (Sanguinetti et al., 1995; Trudeau et al., 1995), and their loss of function can cause arrhythmia. Mutations in *HERG1* (*KCNH2*) or block of hERG1 channels causes long QT syndrome, characterized by prolonged ventricular repolarization and an increased risk of malignant arrhythmia and sudden death (Curran et al., 1995; Keating and Sanguinetti, 2001; Sanguinetti and Tristani-Firouzi, 2006).

The gating of hERG1 channels is modified by divalent cations, including the alkaline earth cations Ca^{2+} and Mg^{2+} (Ho et al., 1998; Johnson et al., 1999b, 2001; Lin and Papazian, 2007), and the transition metal cations Cd^{2+}, Co^{2+}, Ni^{2+}, and Zn^{2+} (Anumonwo et al., 1999; Johnson et al., 1999a; Sanchez-Chapula and Sanguinetti, 2000; Fernandez et al., 2005). The effects of Cd^{2+} on hERG1 channels have been well characterized and were first studied in isolated feline cardiomyocytes, where it was reported to shift the voltage dependence of I_{Kr} activation to more positive potentials and accelerate the rate of current deactivation (Follmer et al., 1992). Later studies of hERG1 channels heterologously expressed in *Xenopus* oocytes determined that Cd^{2+} also slows the rate of activation and produces a positive shift in the voltage dependence of inactivation (Johnson et al., 1999a). Mutations of Asp residues located in the S2 (D456 and D460) and S3 (D509) domains of the hERG1 subunit attenuate the effects of extracellular Cd^{2+} on hERG1 gating, and it has been proposed that together these three acidic residues form a coordination site for Cd^{2+} (Fernandez et al., 2005). These acidic residues, especially D456, also participate in the coordination of Ca^{2+} and Mg^{2+} (Fernandez et al., 2005; Lin and Papazian, 2007). The changes in hERG1 channel gating currents that accompany the altered voltage dependence and

J. Abbruzzese and F.B. Sachse contributed equally to this paper.
Correspondence to M.C. Sanguinetti: sanguinetti@cvrti.utah.edu

Abbreviations used in this paper: COVG, cut-open oocyte Vaseline gap; hERG1, human ether-á-go-go–related gene type 1; VSD, voltage sensor domain; WT, wild type.

The Rockefeller University Press $30.00
J. Gen. Physiol. Vol. 136 No. 2 203–224
www.jgp.org/cgi/doi/10.1085/jgp.201010450

kinetics of ionic currents caused by the binding of divalent cations have not been characterized.

Here, we determine the effects of Cd^{2+} on the gating currents of hERG1 channels heterologously expressed in *Xenopus* oocytes. As expected from previous recordings of ionic currents, Cd^{2+} shifted the OFF gating charge–voltage (Q_{OFF}-V) relationship to more positive potentials and accelerated the decay of OFF gating current (Ig_{OFF}). Cd^{2+} also induced a transient outward current ($I_{Cd\text{-}out}$) upon membrane repolarization from test potentials positive to 0 mV that immediately preceded inward Ig_{OFF}. Other polyvalent metal cations, including Co^{2+}, Zn^{2+}, Ca^{2+}, and La^{3+}, caused a positive shift in the Q_{OFF}-V relationship, but did not induce a similar transient outward current. $I_{Cd\text{-}out}$ was also not observed in D456C or D509C hERG1 channels treated with Cd^{2+} at concentrations that shifted the voltage dependence of channel activation. We propose that $I_{Cd\text{-}out}$ is an ionic current conducted by Cd^{2+} that is displaced from its primary coordination site by Arg residues in S4, as this segment moves inward in response to repolarization of the membrane. The effects of Cd^{2+} were simulated with a new Markov model that describes hERG1 channel gating currents as a noncooperative two-phase process of the voltage sensor domain (VSD).

MATERIALS AND METHODS

Heterologous expression of hERG1 channels in oocytes

HERG1a cDNA (GenBank accession no. NM000328) in the pSP64 plasmid vector (Promega) was linearized with EcoR1, and cRNA was transcribed in vitro with an mMessage mMachine SP6 kit (Applied Biosystems). Mutations were introduced into wild-type (WT) hERG1 using the QuikChange site-directed mutagenesis kit (Agilent Technologies).

Oocytes were isolated by dissection from adult *Xenopus laevis* anaesthetized by immersion in 0.2% tricaine (Sigma-Aldrich) for 10–15 min. After ovarian lobes containing oocytes were removed, the small abdominal incision was sutured closed. Frogs were allowed to recover for at least 1 mo before repeating the surgical procedure to harvest additional oocytes. After a third and final harvest, frogs were anaesthetized with tricaine before pithing. Clusters of oocytes were treated with 2 mg/ml of type 2 collagenase (Worthington) to remove follicle cells. Individual stage IV or V oocytes were microinjected with 5 ng *HERG1* cRNA as described previously (Stühmer, 1992) and incubated in Barth's solution at 19°C for 2–6 d before use in voltage clamp experiments.

Voltage clamp methods

Ionic and gating currents of hERG1 channels were measured by using the cut-open oocyte Vaseline gap (COVG) recording technique (Stefani and Bezanilla, 1998). The COVG chamber consists of three compartments (upper, guard, and bottom) that are isolated from one another by Vaseline seals. Microelectrodes were pulled from borosilicate glass capillary tubes to obtain resistances of 0.1–0.5 MΩ when filled with 3 M KCl and were used to record the transmembrane potential of the oocyte domus protruding into the upper compartment. Electrical access to the cytoplasm was obtained by permeabilizing the portion of the oocyte isolated in the bottom compartment with 0.3% saponin for 2 min. hERG1 channel ionic currents were blocked by adding 10 µM MK-499 (or 10 µM terfenadine in a few experiments) to the upper compartment and tetraethylammonium–methanesulfonic acid (TEA-MES) in all compartments. In addition, to reduce intracellular $[K^+]$, the membrane was initially clamped to 0 mV for 30 min and the solutions in the chamber were exchanged twice.

An amplifier (CA-1B; Dagan), a data acquisition system (Digidata 1322A; MDS Analytical Technologies), and a personal computer were configured to voltage clamp an oocyte with command voltage pulses generated with PCLAMP8 software (MDS Analytical Technologies). Signals were low-pass filtered at 10 kHz and digitized at 40 kHz. Linear leak and capacitance currents were compensated by analogue circuitry and subtracted on-line by using a p/−8 protocol (Armstrong and Bezanilla, 1977). Unless indicated otherwise, the holding potential was −110 mV and the duration of depolarizing test pulses was 300 ms. All recordings were performed at room temperature (22–24°C) under no-flow conditions.

The effects of Cd^{2+} on ionic currents conducted by mutant hERG1 channels were also determined using standard two-microelectrode voltage clamp techniques (Stühmer, 1992), as described previously in detail (Fernandez et al., 2005).

Solutions

Oocytes were incubated in Barth's solution that contained (in mM): 88 NaCl, 1 KCl, 0.4 $CaCl_2$, 0.33 $Ca(NO_3)_2$, 1 $MgSO_4$, 2.4 $NaHCO_3$, 10 HEPES, and 1 pyruvate, pH 7.4, supplemented with 50 µg/ml gentamycin. Ionic currents were recorded using an extracellular solution in the top and guard compartments that contained (in mM): 96 NaCl, 4 KCl, 1 $CaCl_2$, 1 $MgCl_2$, and 5 HEPES; pH adjusted to 7.6 with NaOH. The same solution was used to bathe oocytes that were voltage clamped using the standard two-microelectrode voltage clamp technique. The extracellular solution in the top and guard compartments for measurement of gating currents contained (in mM): 120 TEA-MES, 2 Ca-MES, and 10 HEPES, pH 7.4. The intracellular solution in the bottom compartment contained (in mM): 120 TEA-MES, 2 EDTA, and 10 HEPES, pH 7.4. $CdCl_2$ was obtained from Sigma-Aldrich. No compensation was made for Cd^{2+} binding to HEPES (Cherny and DeCoursey, 1999). RPR260243, a hERG1 channel activator (Kang et al., 2005), was provided by Sanofi-Aventis Pharmaceuticals and prepared for use by dilution of a 10-mM DMSO stock solution.

Data analysis

pCLAMP8 (MDS Analytical Technologies) and Origin 7.5 (OriginLab) were used for off-line data analysis. Integration of the OFF gating current (Ig_{OFF}) induced by subsequent repolarization was used to calculate the OFF intramembrane charge displacement (Q_{OFF}). Accurate measurement of ON intramembrane charge displacement (Q_{ON}) was difficult because nonlinear and/or time-dependent leak and endogenous currents activated at the more positive test potentials could not be adequately subtracted with the p/−8 pulse protocol. The charge–voltage (Q_{OFF}-V) relationship for each oocyte, defined by the plot of Q_{OFF} measured at −110 mV versus test potential (V_t), was normalized to the calculated maximum value ($Q_{OFF\text{-}max}$) determined from fitting the data to a Boltzmann function:

$$\frac{Q_{OFF}}{Q_{OFF-\max}} = \frac{1}{1+e^{-\frac{zF}{RT}(V_t-V_{1/2})}}, \quad (1)$$

where $V_{1/2}$ is the half-point of the relationship, z is the effective valence, and RT/F is 25.4 mV at 22°C. The onset of the extracellular Cd^{2+}-induced alteration of gating currents required only a few minutes to reach a steady state. However, continued exposure to solutions with $[Cd^{2+}]_e > 100$ µM slowly reduced the peak

magnitude of Q_{OFF}. To compensate for this effect, the Q_{OFF}-V relationship for each cell was normalized to the extrapolated maximum Q_{OFF} value determined for each $[Cd^{2+}]_e$. The G-V relationship for ionic currents, defined by the plot of G/G_{max} versus test potential, was also fitted to a Boltzmann function.

Modeling of gating currents

Two Markov models of hERG1 channel currents were developed to reconstruct experimental data without Cd^{2+} (standard model) and with Cd^{2+} (Cd^{2+} model). Each model includes two components, one for the voltage sensing (Figs. 13 A and 17) and the other for activation and inactivation (Fig. 13 B). The models differ in the topology of their VSD component. The standard model is based on a topology that has been previously developed to describe the gating currents of Shaker (Zagotta et al., 1994) and hERG1 channels (Piper et al., 2003). The Cd^{2+} model extends the standard model by incorporating states and transitions describing the movements of Cd^{2+} in the VSD of hERG1 (Fig. 17). Based on the effect of 100 µM Cd^{2+} on the measured Q-V relationship (Fig. 2), we assumed that at this $[Cd^{2+}]_e$, two Cd^{2+} are bound per channel, each to a single site in the VSD of a subunit. Thus, the model allows for two Cd^{2+} movements per channel. In general, forward rates α_{ij} and backward rates β_{ij} between the i-th and j-th state were defined as dependent on the transmembrane voltage V_m:

$$\alpha_{ij} = \alpha_{ij,o} e^{z_{ij,\alpha}\frac{V_m F}{RT}} \tag{2}$$

$$\beta_{ij} = \beta_{ij,o} e^{z_{ij,\beta}\frac{V_m F}{RT}}, \tag{3}$$

with the rates $\alpha_{ij,0}$ and $\beta_{ij,0}$ at 0 mV, the charges $z_{ij,\alpha}$ and $z_{ij,\beta}$, the temperature T, Faraday constant F, and the gas constant R. The rates between the states C_0 and C_1 were defined as a function of states S_i in the VSD component:

$$\alpha_{C0C1} = \alpha_{o,C0C1}\left(S_4 + S_8 + S_{11} + S_{13} + S_{14}\right) \quad \text{(4; standard model)}$$

$$\alpha_{C0C1} = \alpha_{o,C0C1}\left(\begin{array}{c} S_4 + S_8 + S_{11} + S_{13} + S_{14} \\ + S_{18} + S_{21} + S_{23} + S_{24} + S_{27} + S_{29} + S_{30} \end{array}\right) \quad \text{(5; } Cd^{2+} \text{ model)}$$

$$\beta_{C0C1} = \beta_{o,C0C1} \tag{6}$$

The gating current of hERG1 channels was defined as the sum of gating currents $Ig_{ij,g}$ associated with transitions between the i-th and j-th state:

$$Ig = \sum_{ij} Ig_{ij} \tag{7}$$

In general, the gating current associated with transitions between the state S_i and state S_j was described as:

$$Ig_{ij} = \left(z_{ij,\alpha} + z_{ij,\beta}\right)\left(S_i\alpha_{ij} - S_j\beta_{ij}\right) \tag{8}$$

In the Cd^{2+} model, the gating current was extended by a current I_{Cd} related to Cd^{2+} movement:

$$I_{Cd} = \sum_{ij} z_{Cd}\left(S_i\alpha_{ij} - S_j\beta_{ij}\right), \tag{9}$$

with the charge z_{Cd} associated to the movement of Cd^{2+} opposite to the transmembrane electric field. Rates associated with Cd^{2+} movement in the VSD (μ_{ij} and η_{ij}; Fig. 17) were defined as voltage dependent, as described in Eqs. 2 and 3. Parameters of the Markov models were determined by numerical fitting of feature vectors extracted from experimental and model data, f_e and f_m, respectively. The fit error E was defined as:

$$E = \sqrt{\sum_{i=1\ldots n}\left(\frac{\left\| f_{m,i} - f_{e,i}\right\|_2}{\left\| f_{e,i}\right\|_2}\right)^2 + \left(1 - Max\, S_{14,ON}\right)^2 + \left(Min\, S_{14,OFF}\right)^2}, \tag{10}$$

with the number of features n, the Euclidean norm $\|\ldots\|_2$, the maximum of the state S_{14} during the test pulses Max $S_{14,ON}$, and the minimum of S_{14} after the test pulses Min $S_{14,OFF}$. Features included Q-V relationships and parameters from exponential fits of Ig_{ON} and Ig_{OFF} at different voltages (Table S1). The fit error E included functions of Max $S_{14,ON}$ and Min $S_{14,OFF}$ to select parameter sets that cause high state probabilities of S_{15} at activating voltages and low probability of S_{15} at deactivation, respectively. The fitting procedure was iterative and combined random perturbation and selection of parameter sets causing the smallest fit error followed by their optimization. The number of iterations was 80. In each iteration, 1,600 perturbed parameter sets were evaluated. Perturbations were initially in the range of 1–200% of the original parameter value. The perturbation range was decreased in each iteration to a final range of 99.9–100.1%. The 64 parameter sets with the smallest fit error were optimized using the steepest descent method (Press et al., 1992) and used for the parameter set perturbation in the next step. Fitting of the Cd^{2+} model was based on parameters of the standard model. The sum of z_α and z_β (charge associated with fast transitions), as well as of z_γ and z_δ (charge associated with slow transitions), was kept the same in the standard and Cd^{2+} models.

The simulations were performed with a variable order method for solution of ordinary differential equations based on numerical differentiation formulas (Matlab function: ode15s). An initial time step Δt of 10 fs was chosen. For both models, the temperature was set at 296°K. All calculations were performed in double precision. All software was developed with Matlab 7.9 (The MathWorks Inc.). Numerical fitting procedures were accelerated by using the Matlab Parallel Computing Toolbox.

Online supplemental material

Table S1 lists fit errors for model fitting of Q-V relationships and kinetics of Ig_{ON} and Ig_{OFF}. Table S2 presents the initial values for channel states of the standard and Cd^{2+} models. Table S3 lists the rate constant parameters for the standard and Cd^{2+} models. The online supplemental material is available at http://www.jgp.org/cgi/content/full/jgp.201010450/DC1.

RESULTS

Cd^{2+} shifts the voltage dependence of hERG1 channel gating

hERG1 channel gating currents were elicited with 300-ms depolarizations to test potentials that ranged from −100 to +60 mV. Outward ON gating currents (Ig_{ON}) were detectable for depolarizations to test potentials positive to −70 mV, and inward OFF gating currents (Ig_{OFF}) were induced upon subsequent repolarization to the holding potential of −110 mV. An example of

currents recorded from a control oocyte (not injected with cRNA) at a test potential of +60 mV is shown in Fig. 1 A. In this and four other oocytes examined, no gating currents were observed before or after treatment with 30 μM Cd^{2+}. Fig. 1 B shows currents recorded at test potentials of −10, +10, and +60 mV in an oocyte previously injected with hERG1 cRNA. In this cell, depolarizing pulses elicited a transient outward gating current (Ig_{ON}) composed of rapid and slow components. Repolarization to −110 mV also elicited rapid and slow components of inward gating current (Ig_{OFF}). At increasingly positive test potentials, the slow component of Ig_{ON} became more apparent and the fast component of Ig_{OFF} was reduced. In addition, a very small transient outward current that preceded the large inward Ig_{OFF} was measured upon repolarization to −110 mV from the pulse to +60 mV. This tiny outward current could represent a bona fide reduction in capacitance caused by a decrease in polarizability (Sigworth, 1994) or an artifact of the p/−8 subtraction procedure (Stühmer et al., 1991). The same oocyte was then exposed to 30 μM Cd^{2+} for 10 min before gating currents were again recorded at the same test potentials (Fig. 1 C). Cd^{2+} reduced the magnitude of the slow component of Ig_{ON} at all test potentials and reduced the fast component of Ig_{ON} at +10 and +60 mV. Note that in the presence of 30 μM Cd^{2+}, the magnitude and kinetics of Ig_{ON} at +60 mV nearly matched Ig_{ON} recorded at +10 mV under control conditions, consistent with a Cd^{2+}-induced positive shift in the voltage dependence of channel activation. The most obvious effect of Cd^{2+} was the appearance of a large transient outward current that immediately preceded Ig_{OFF}. This Cd^{2+}-induced outward current associated with membrane repolarization is hereafter referred to as $I_{Cd\text{-}out}$.

The Q_{OFF}-V relationship was determined for the same oocytes under control ionic conditions and in the presence of extracellular solutions containing [Cd^{2+}] that was varied from 3 to 300 μM. Cd^{2+} induced a concentration-dependent positive shift of $V_{1/2}$ and a reduction in the slope of the Q_{OFF}-V relationship (Fig. 2 A). The shift in $V_{1/2}$ of the Q_{OFF}-V relationship measured from gating currents and the G-V relationship measured from ionic currents are plotted as a function of $[Cd^{2+}]_e$ in Fig. 2 B. For both the Q_{OFF}-V and G-V plots, the maximum Cd^{2+}-induced shift in $V_{1/2}$ ($\Delta V_{1/2max}$) was set at +90 mV, the value determined from extrapolation of the averaged $\Delta V_{1/2}$ for the G-V dataset. The EC_{50} for the Cd^{2+}-induced shift in $V_{1/2}$ for the Q_{OFF}-V relationship was 171 ± 13 μM with a Hill coefficient, n_H, of 0.53 ± 0.03. The EC_{50} for the Cd^{2+}-induced shift in $V_{1/2}$ for the G-V relationship was ~2.4 times greater (416 ± 20 μM), but the Hill coefficient was similar (n_H = 0.57 ± 0.02). The effects of Cd^{2+} on the values of $V_{1/2}$ and z determined from fitting these data to a Boltzmann function are summarized in Fig. 2 (C and D, respectively). The [Cd^{2+}]-dependent reduction in z likely results from a slowing of Ig_{ON} and incomplete charge displacement during the 300-ms test pulse for intermediate depolarizations. Thus, Cd^{2+} induced a concentration-dependent positive shift in the Q_{OFF}-V relationship for hERG1, an effect that was 2.4 times more potent than the voltage-dependent shift of the G-V relationship for ionic currents.

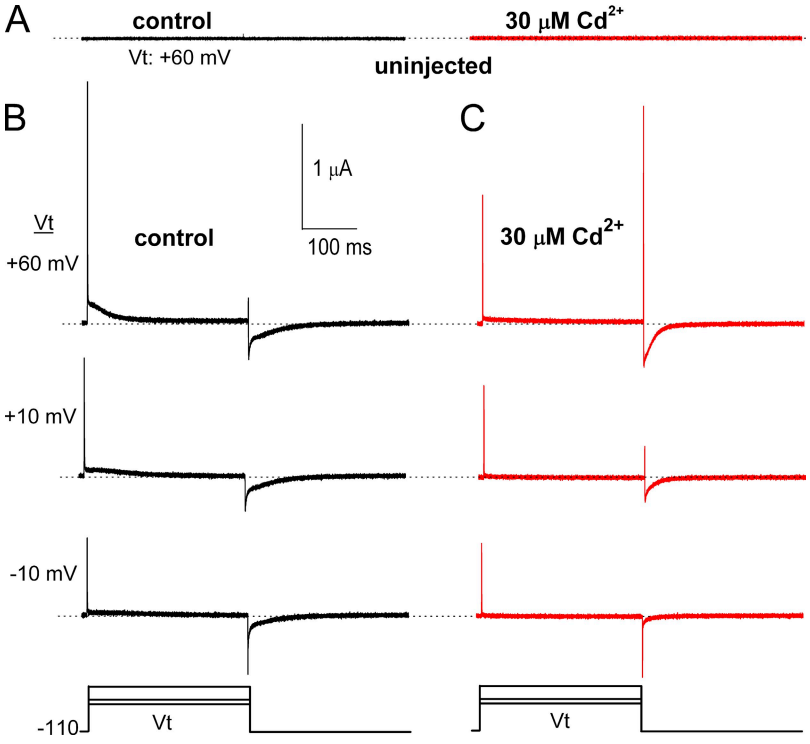

Figure 1. Effect of Cd^{2+} on hERG1 channel gating currents. (A) Currents recorded at a V_t of +60 mV using the COVG technique from an uninjected oocyte before (control) and 10 min after bath application of 30 μM Cd^{2+}. Recordings were made with the same solutions used to record gating currents in oocytes expressing hERG1 channels. (B and C) Gating currents recorded at the indicated V_t before and after treatment of the same oocyte with 30 μM Cd^{2+}. Bottom panels illustrate voltage clamp protocol used to elicit gating currents shown in panels A–C.

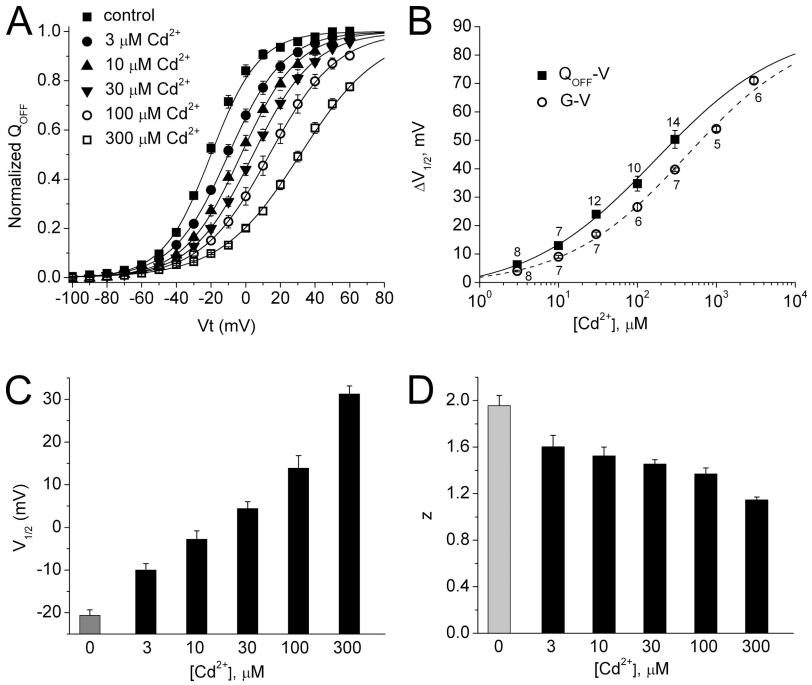

Figure 2. Extracellular Cd^{2+} shifts the Q-V relationship for hERG1 to more positive potentials. (A) Normalized Q_{OFF} is plotted as a function of V_t and $[Cd^{2+}]_e$. Averaged data for control and each $[Cd^{2+}]_e$ were fitted to a Boltzmann function (smooth curves). (B) Plot of change in $V_{1/2}$ for Q-V and G-V relationships as a function of $[Cd^{2+}]_e$. Data were fitted to a Hill equation to determine EC_{50} and Hill coefficient (n_H). $\Delta V_{1/2max}$ was set at +90 mV (Fernandez et al., 2005). For Q-V relationship, EC_{50} = 171 ± 13 μM; n_H = 0.53 ± 0.03. For G-V relationship, EC_{50} = 416 ± 20 μM; n_H = 0.57 ± 0.02. The number of oocytes used to calculate the average data is indicated next to each data point. (C) $[Cd^{2+}]_e$-dependent effects on $V_{1/2}$ for Q-V relationship. (D) $[Cd^{2+}]_e$-dependent effects on effective valence, *z*, of Boltzmann function for Q-V relationship. For A, C, and D, the number of oocytes was as follows: control, 20; 3 μM Cd^{2+} , 8; 10 μM Cd^{2+}, 7; 30 μM Cd^{2+}, 12; 100 μM Cd^{2+}, 10; 300 μM Cd^{2+}, 14.

To facilitate viewing the effects of Cd^{2+} on the multiple components of gating currents, traces for currents elicited in response to a test pulse to +40 mV before and after treatment of an oocyte with 30 μM Cd^{2+} are superimposed in Fig. 3. Cd^{2+} reduced the amplitude of both the rapid initial component and the slow component of Ig_{ON}, and it altered the kinetics of Ig_{OFF} (Fig. 3 A). The initial 9 ms of Ig_{ON} traces recorded during control conditions and after treatment of an oocyte with 30 μM Cd^{2+} are shown in Fig. 3 B. The time to peak outward Ig_{ON} was decreased from 430 to 300 μs by Cd^{2+}, and the magnitude of the slow component was reduced, consistent with the positive shift in the voltage dependence of gating (Fig. 2). The initial 9 ms of Ig_{OFF} traces recorded during control conditions and after treatment of an oocyte with 30 μM Cd^{2+} are shown in Fig. 3 C. Cd^{2+} induced a large outward component of Ig_{OFF} and slightly prolonged the time to peak of inward Ig_{OFF}.

Characterization of $I_{Cd\text{-}out}$

Cd^{2+} did not induce $I_{Cd\text{-}out}$ in uninjected oocytes (Fig. 1 A), indicating that this current does not represent some unidentified Cd^{2+}-activated endogenous current or nonlinear capacitance current. Nonetheless, with a time to peak of <240 μs, the obvious concern is that $I_{Cd\text{-}out}$ represents an experimental artifact resulting from the leak and capacitance current subtraction protocol. When using p/−8 subtraction, we never observed an inward transient at the start of the depolarizing pulse, arguing against poor compensation as a potential problem. We also measured gating currents in oocytes where the capacitance current was compensated by analogue circuitry only, without p/−8 on-line leak subtraction (Fig. 4, A and B). For this oocyte, a normal shift in the Q_{OFF}-V relationship was observed (Fig. 4 C), as well as a large $I_{Cd\text{-}out}$ after pulsing to positive potentials (Fig. 4 D).

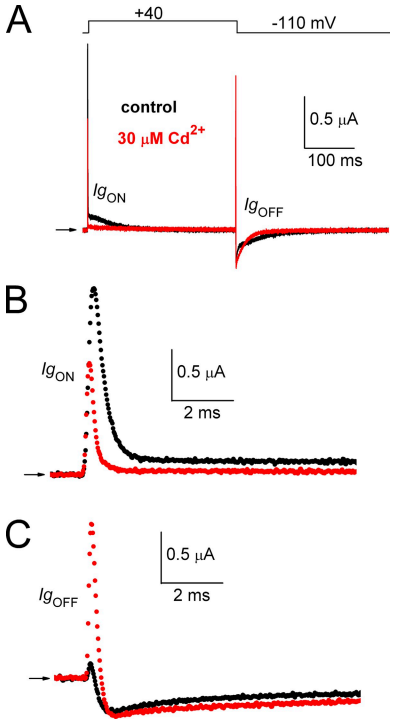

Figure 3. Cd^{2+} reduces the fast and slow components of Ig_{ON} and induces the appearance of $I_{Cd\text{-}out}$, a brief initial outward component that precedes Ig_{OFF}. (A) Superimposed traces for gating currents measured before and after treatment of an oocyte with 30 μM Cd^{2+}. Top panel shows pulse protocol. (B) Ig_{ON} shown on an expanded time scale. (C) Ig_{OFF} shown on an expanded time scale.

The time course of $I_{Cd\text{-}out}$ determined in the cell using p/−8 subtraction (Fig. 4 E, blue trace) coincided in time and approximate peak magnitude with the current measured without the use of the p/−8 subtraction protocol (Fig. 4 E, red trace). To be certain that $I_{Cd\text{-}out}$ was not an artifact arising from subtraction of a rapid component of Ig_{ON} that activated at test potentials negative to the holding potential of −110 mV, we confirmed that no Ig_{ON} was present for pulses applied to test potentials between −140 and −100 mV from a holding potential of −150 mV (not depicted).

The relative magnitude of the charge associated with the outward component of Ig_{OFF} (Q_{out}) under control ionic conditions and $I_{Cd\text{-}out}$ ($Q_{Cd\text{-}out}$) in the presence of Cd^{2+} compared with Q_{OFF} was determined for test potentials ranging from 0 to +60 mV and for $[Cd^{2+}]_e$ ranging from 3 to 300 µM. Fig. 5 (A and B) illustrates how the $I_{Cd\text{-}out}$ and inward Ig_{OFF} were defined for this comparison, and Fig. 5 C shows the integration of the two current components. The peak outward component of Q_{OFF} was defined as $Q_{Cd\text{-}out}$, and the peak of the inward component of Q_{OFF} was defined as $Q_{OFFtotal}$. Under control ionic conditions, $Q_{Cd\text{-}out}$ was very small, equivalent to ∼0.3% of $Q_{OFFtotal}$ for a V_t of +40 mV. Cd^{2+} increased the relative magnitude of $Q_{Cd\text{-}out}$ at all test potentials in a concentration-dependent manner for 3–100 µM Cd^{2+} (Fig. 5 D). At 300 µM, the voltage dependence of $Q_{Cd\text{-}out}/Q_{OFFtotal}$ was right-shifted and therefore reduced compared with 100 µM Cd^{2+}. Fig. 5 E is a plot of $Q_{Cd\text{-}out}/Q_{OFF}$ as a function of V_t for 100 µM Cd^{2+}. The maximum value of $Q_{Cd\text{-}out}/Q_{OFFtotal}$ was estimated to be 0.064. Thus, even at high $[Cd^{2+}]_e$, $Q_{Cd\text{-}out}$ is a very minor component of the total Q_{OFF}.

Finally, we determined if the increase in the magnitude of $Q_{Cd\text{-}out}$ and Q_{OFF} followed a similar time course. This was accomplished by pulsing to +60 mV for a variable time and plotting the integrals of $I_{Cd\text{-}out}$ and Ig_{OFF} as a function of pulse duration. Fig. 6 A shows control gating currents (top traces) elicited with test pulses of variable duration to +60 mV. The middle traces illustrate the pulse protocol, and the bottom traces show the corresponding integrals of Ig_{OFF}. Fig. 6 B shows gating currents and their integrations after exposure of the same oocyte to 30 µM Cd^{2+}. The values of Q_{OFF} were plotted as a function of pulse duration, and the data were fitted to an exponential function (Fig. 6 C). The time constant for the increase in Q_{OFF} by pulse duration was 29 ms in control and was slowed to 100 ms in the presence of Cd^{2+}. After an initial delay of ∼50 ms, presumably caused by a masking of $I_{Cd\text{-}out}$ by the overlapping large fast inward component of Ig_{OFF}, $Q_{Cd\text{-}out}$ was increased exponentially with a time constant of 95 ms (Fig. 6 D). The average time constant for the increase of peak Q_{OFF} in four oocytes was 107 ± 14 ms in the presence of Cd^{2+}.

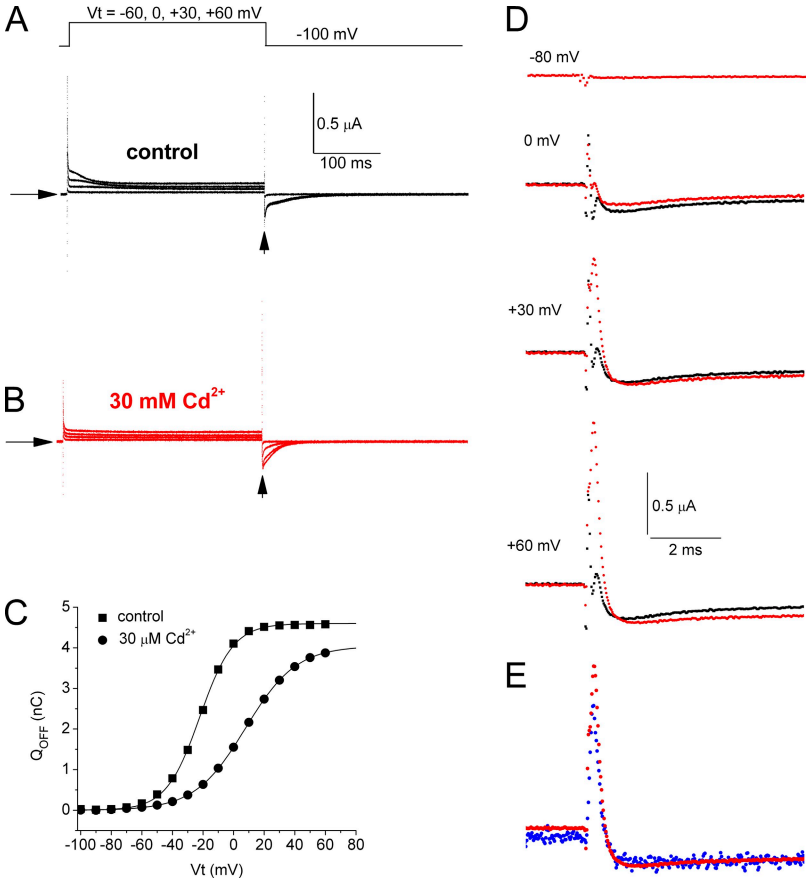

Figure 4. Gating currents measured without using p/−8 leak and capacitance current subtraction. (A) Unsubtracted currents recorded under control ionic conditions using pulse protocol illustrated in top panel. (B) Unsubtracted currents for the same oocyte in the presence of 30 µM Cd^{2+}. (C) Q_{OFF}-V relationships for gating currents recorded in the absence and presence of 30 µM Cd^{2+}. Data were fitted to a Boltzmann function (smooth curves). In control conditions, $V_{1/2}$ = −22.1 mV and z = 2.29. In the presence of Cd^{2+}, $V_{1/2}$ = +7.8 mV and z = 1.52. (D) Superimposed traces of unsubtracted Ig_{OFF} for control (black traces) and 30 µM Cd^{2+} (red traces) at −110 mV after activating pulses were applied to the indicated V_t. (E) Superimposed traces for p/−8 subtracted (blue) and unsubtracted currents (red) in the presence of 30 µM Cd^{2+} for a V_t of +60 mV. Note that $I_{Cd\text{-}out}$ is approximately the same, indicating that it is not an artifact of the on-line leak subtraction protocol.

Thus, the time course for increase in $Q_{Cd\text{-}out}$ as a function of pulse duration matches reasonably well with the increase in Q_{OFF}.

Effect of extracellular Co^{2+}, Zn^{2+}, La^{3+}, and elevated $[Ca^{2+}]_e$ on hERG1 gating currents

Similar to the effects of Cd^{2+}, elevation of $[Ca^{2+}]_e$ causes a positive shift in the G-V relationship of hERG1 (Ho et al., 1998; Johnson et al., 1999b). As expected, the elevation of $[Ca^{2+}]_e$ from 2 to 10 mM shifted the Q_{OFF}-V relationship by +26 mV; however, unexpectedly, $Q_{OFF\text{-}max}$ was increased by 44% (Fig. 7 A). The increase in $Q_{OFF\text{-}max}$ was reversible upon return to a lower $[Ca^{2+}]_e$. Unlike Cd^{2+}, the shift in the Q_{OFF}-V relationship by Ca^{2+} was not associated with the appearance of a brief outward current upon repolarization to −110 mV. In fact, 10 mM Ca^{2+} eliminated the small outward transient (Fig. 7, B and C), probably because it was masked by the accelerated rate of onset of inward Ig_{OFF}.

The effect of the addition of Cd^{2+} in the continued presence of 10 mM Ca^{2+} is illustrated in Fig. 7 (D–G). Although no outward component of Ig_{OFF} is visible with 10 mM Ca^{2+}, the addition of 100 µM Cd^{2+} induced the appearance of $I_{Cd\text{-}out}$ (Fig. 7, D and E). These changes reflect altered hERG1 gating because no rapid currents were induced in uninjected oocytes treated with these concentrations of Ca^{2+} or Cd^{2+} (Fig. 7 F). The addition of Cd^{2+} reduced $Q_{OFF\text{-}max}$ to nearly the same level measured with 2 mM Ca^{2+} and shifted the $V_{1/2}$ of the Q_{OFF}-V relationship by a further +25 mV (Fig. 7 G). Normally, 0.1 mM Cd^{2+} causes a +35-mV shift in the Q_{OFF}-V relationship (Fig. 2). The reduced shift in $V_{1/2}$ and the reduction in $Q_{OFF\text{-}max}$ caused by Cd^{2+} in the continuous presence of 10 mM Ca^{2+} indicate that the effects of Ca^{2+} and Cd^{2+} were not additive, consistent with competition for the same or overlapping binding site. The same effects of elevated $[Ca^{2+}]_e$ and the subsequent addition of 100 µM Cd^{2+} were observed in five oocytes.

Other divalent transition metal cations such as Co^{2+} (Sanchez-Chapula and Sanguinetti, 2000) or Zn^{2+} (Anumonwo et al., 1999), or the trivalent La^{3+} (Sanchez-Chapula and Sanguinetti, 2000), also cause a positive shift in the G-V relationship of hERG1. Therefore, we characterized the effects of these three cations at concentrations chosen to match the +35-mV shift in the Q_{OFF}-V relationship caused by 100 µM Cd^{2+} that also induced the maximal increase in $I_{Cd\text{-}out}$. Co^{2+} at 3 mM shifted Q_{OFF}-V by +35 mV, with only a slight change in effective valence (z) and without changing the peak value of Q_{OFF} (Fig. 8 A). However, similar to Ca^{2+} and unlike Cd^{2+}, Co^{2+} eliminated the small outward transient present under control conditions (Fig. 8, B and C). Zn^{2+} at 1 mM shifted Q_{OFF}-V by +34 mV, but it also reduced z for this relationship and reduced $Q_{OFF\text{-}max}$ by ∼20% (Fig. 8 D). However, unlike Cd^{2+}, Ca^{2+}, or Co^{2+}, Zn^{2+} did not appreciably alter the initial kinetics of Ig_{OFF} or alter the amplitude of its brief

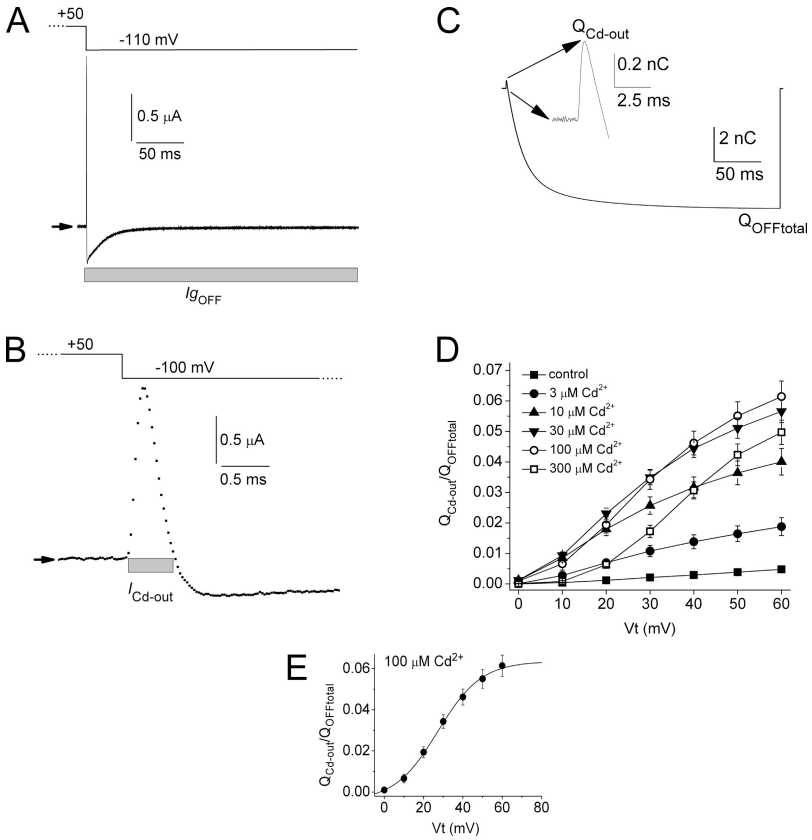

Figure 5. Effect of $[Cd^{2+}]_e$ on the magnitude of $I_{Cd\text{-}out}$. (A) Ig_{OFF} in the presence of 30 µM Cd^{2+}. Arrows indicate zero current level. Gray bar indicates region of Ig_{OFF} integrated to obtain total Q_{OFF}. (B) $I_{Cd\text{-}out}$ shown in A, plotted on an expanded time scale. Gray bar indicates the region of Ig_{OFF} integrated to obtain $Q_{Cd\text{-}out}$. (C) Integral of Ig_{OFF}. Inset shows Q_{OFF} at greater resolution. (D) Plot of $Q_{Cd\text{-}out}/Q_{OFF}$ total as a function of V_t and $[Cd^{2+}]_e$. Also shown is a plot of $Q_{Cd\text{-}out}$ versus V_t for control conditions. (E) Plot of $Q_{Cd\text{-}out}/Q_{OFF}$ total as a function of V_t for 100 µM Cd^{2+} and fitted to a Boltzmann function (smooth curve): $V_{1/2}$ = 27 mV; slope factor = 11.0 mV; maximum value of $Q_{Cd\text{-}out}/Q_{OFF}$ total = 0.064.

outward component (Fig. 8, E and F). La^{3+} at a concentration of 10 μM caused a +40-mV shift of the Q_{OFF}-V relationship, reduced z, and reduced $Q_{OFF\text{-}max}$ by ∼20% (Fig. 8 G), mirroring the effects of Zn^{2+}. However, like Ca^{2+} and Co^{2+}, the brief outward current associated with repolarization was absent in the presence of La^{3+}, presumably because it was obscured by the rapid onset of inward Ig_{OFF} (Fig. 8, H and I).

In summary, a transient outward current associated with repolarization was: only observed in oocytes expressing hERG1 channels; increased as a function of $[Cd^{2+}]_e$, and the charge carried by this current ($Q_{Cd\text{-}out}$) increased in magnitude as a function of test pulse duration similar to Q_{OFF}; and not observed in oocytes treated with Co^{2+}, La^{3+}, or elevated $[Ca^{2+}]_e$.

$I_{Cd\text{-}out}$ is eliminated by neutralization of acidic residues in the S2 or S3 segment

The hERG1 subunit contains two acidic residues in S2 (D456 and D460) and one in S3 (D509) that together constitute the primary components of a putative binding site for extracellular applied Cd^{2+} (Fernandez et al., 2005). Assuming that a Cd^{2+} ion bound to a coordination site is within the transmembrane electric field, its outward displacement in response to membrane repolarization could produce $I_{Cd\text{-}out}$. Conceivably, Cd^{2+} movement could result from its unbinding from a unique coordination site, or by a change in the highly localized electrostatics of the binding site (e.g., altered interaction with one or more of the Asp residues in S2 or S3). Mutation of the key acidic residues in S2 or S3 could alter the coordination chemistry of this putative Cd^{2+} binding site and potentially alter the properties of $I_{Cd\text{-}out}$. We previously reported that mutation of D456, D460, or D509 to Ala shifted the voltage dependence of hERG1 channel activation to more positive potentials and greatly attenuated the effects of Cd^{2+} on the gating of ionic currents (Fernandez et al., 2005). Here, we instead mutated these residues to Cys to neutralize their negative charge while retaining their ability to coordinate Cd^{2+}.

Ionic and gating currents were recorded from D456C and D509C channels, but D460C channels did not express at sufficient levels to permit recording of gating currents and were not further characterized. We first characterized the effect of the single Cys mutations on hERG1 ionic currents. The $V_{1/2}$ of the G-V relationship for D509C ionic currents activated with 5-s test pulses was 6.6 ± 0.7 mV (z = 1.89 ± 0.06; n = 5), a shift of +42 mV compared with WT hERG1 ($V_{1/2}$ = −35.0 ± 0.3 mV; z = 3.5 ± 0.1; n = 14). Cd^{2+} at 1 mM shifted the $V_{1/2}$ for activation of D509C hERG1 ionic currents by an additional +34.4 ± 0.3 mV (n = 5; Fig. 9 A), similar to the +36-mV shift produced with 0.5 mM Cd^{2+} on WT hERG1 channels under identical conditions (Fernandez et al., 2005). The $V_{1/2}$ for activation of D456C hERG1 channel

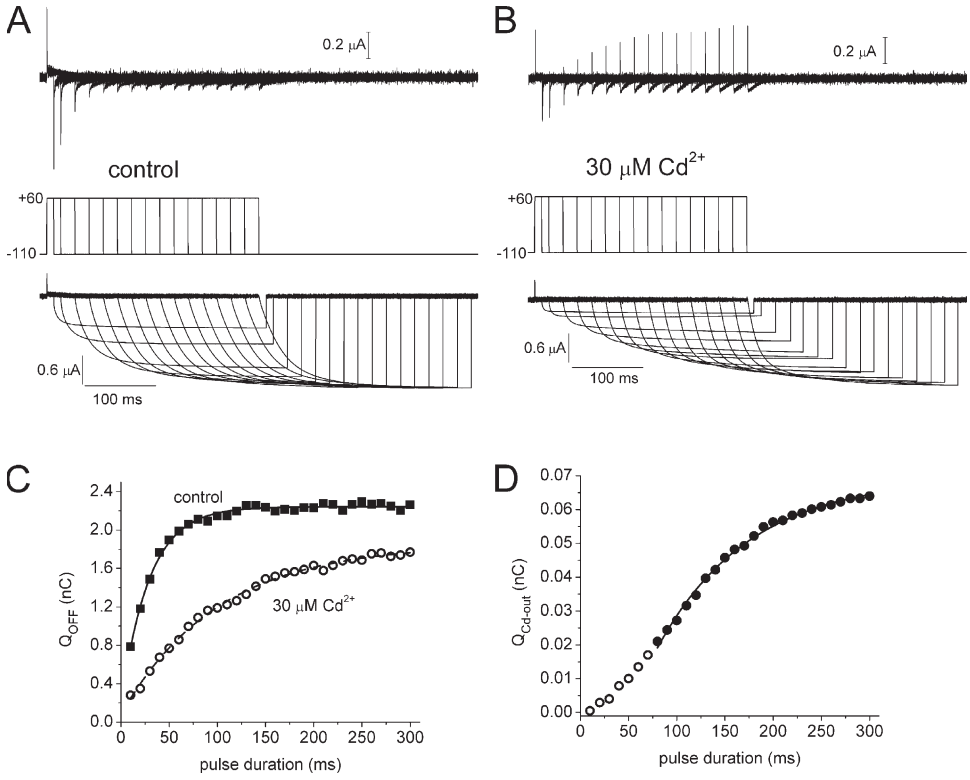

Figure 6. Kinetics of Q_{OFF}. (A) Gating currents elicited under control conditions. Top panel is a plot of gating currents in response to voltage pulse protocol shown in the middle panel. Bottom panel shows the first integral of Ig_{OFF} traces depicted in top panel. (B) Gating currents, pulse protocol, and integration of currents are shown for the same oocyte after bath application of 30 mM Cd^{2+}. (C) Plot of total Q_{OFF} versus pulse duration determined before (filled squares) and after treatment of an oocyte with Cd^{2+} (open circles). Smooth curves are best fits for single-exponential function (τ = 29 ms for control; τ = 100 ms for Cd^{2+}). (D) Plot of $Q_{Cd\text{-}out}$ in the presence of 30 μM Cd^{2+} versus pulse duration. Data for pulse durations >70 ms (filled circles) were fitted with a single-exponential function (τ = 95 ms). Thus, after accounting for a delay caused by overlap of the faster rising phase of Ig_{OFF} for short pulse durations, the time course of the development of $Q_{Cd\text{-}out}$ matches that of Q_{OFF}.

ionic currents was 5.1 ± 3.4 mV (z = 1.89 ± 0.11; n = 8), a shift of +40 mV compared with WT hERG1. Cd^{2+} at 1 mM shifted the $V_{1/2}$ for activation of D456C hERG1 channels by +34.4 ± 2.2 mV (n = 5; Fig. 9 B). Thus, both D456C and D509C mutant hERG1 channels retained high sensitivity to Cd^{2+}, albeit reduced by twofold compared with WT hERG1.

For WT hERG1, the $Q_{Cd\text{-}out}/Q_{OFF}$ ratio was most prominent at 100 µM Cd^{2+} (Fig. 5 D). Considering the approximately twofold lower potency of Cd^{2+} on the ionic currents of D456C and D509C hERG1, we used 0.3 mM Cd^{2+} to maximize the chances of observing $I_{Cd\text{-}out}$ in these mutant channels. Cd^{2+} shifted the Q_{OFF}-V relationship to more positive potentials and accelerated the onset and decay of Ig_{OFF} for D509C and D456C channels. For D509C, $V_{1/2}$ was +49.6 ± 4.5 mV (z = 0.76 ± 0.06) during control and +86.8 ± 1.5 mV (z = 0.73 ± 0.03) in the presence of 0.3 mM Cd^{2+}, a shift of +37 mV (n = 4). For D456C, $V_{1/2}$ was +28.0 ± 1.7 mV (z = 0.79 ± 0.05) during control and +62.5 ± 2.5 mV (z = 0.85 ± 0.05) after 0.3 mM Cd^{2+}, a shift of +34.5 mV (n = 3; not depicted). However, in contrast to WT hERG1 (Fig. 10 A), Cd^{2+} did not induce the appearance of $I_{Cd\text{-}out}$ in the two mutant hERG1 channels. Examples of Ig_{OFF} activated by repolarization from a V_t ranging from +30 to +90 mV (or +20 to +80 mV), applied in 20-mV increments, are shown in Fig. 10 B for D509C and Fig. 10 C for D456C channels. These specific test potentials are +30 or +40 mV positive to the voltages used to elicit Ig_{OFF} for WT channels (Fig. 10 A) and represent equivalent stimuli, taking into consideration the shift in the voltage dependence of activation induced by the specific Cys substitutions. Thus, similar to WT hERG1 channels, Cd^{2+} shifted the voltage dependence of activation and accelerated the decay of Ig_{OFF} of D509C and D456C channels. However, unlike in WT channels, Cd^{2+} did not induce the appearance of $I_{Cd\text{-}out}$ in these mutant channels.

Markov models of hERG1 channel gating and gating currents

For most voltage-gated ion channels, the intramembrane displacement of charge that produces a gating

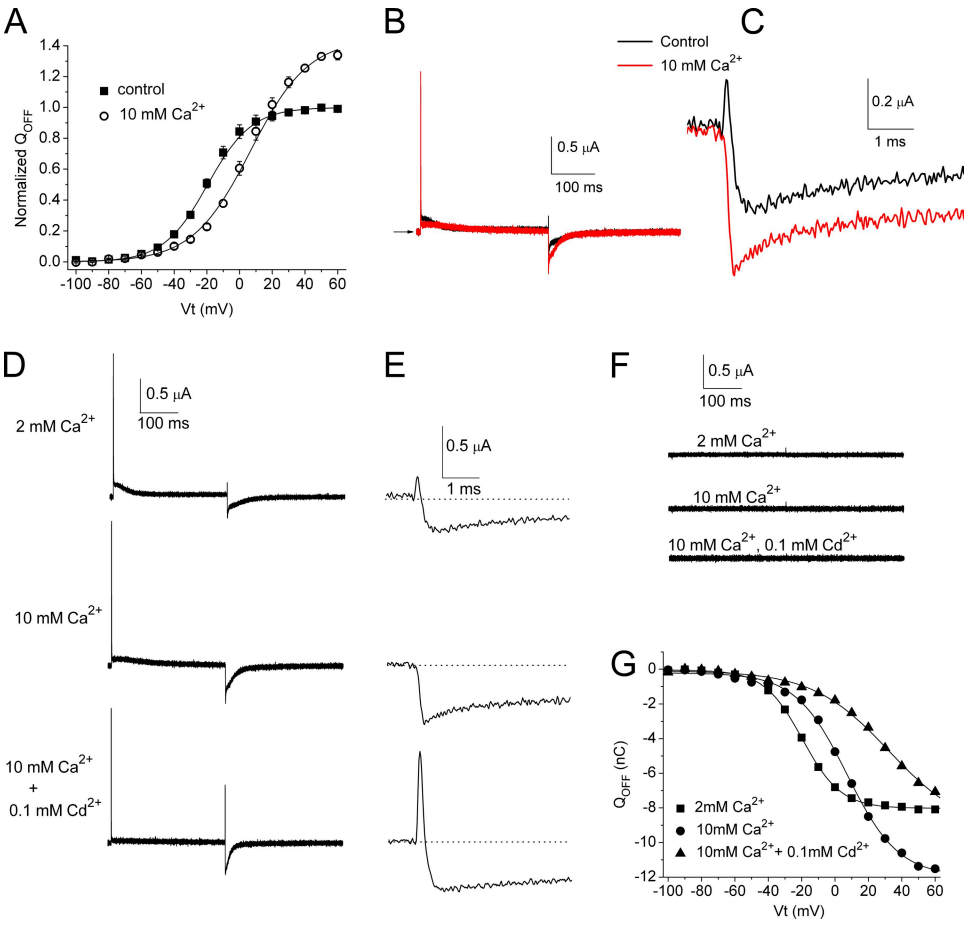

Figure 7. Elevated concentration of Ca^{2+} causes a positive shift in the voltage dependence of the Q_{OFF}-V relationship for hERG1, but it does not induce a transient outward component in Ig_{OFF}. (A) Q_{OFF}-V relationships for hERG1 measured under control conditions ($[Ca^{2+}]_e$ = 2 mM) and after the elevation of $[Ca^{2+}]_e$ to 10 mM (n = 5). Averaged data were fitted to a Boltzmann function (smooth curves). 2 mM Ca^{2+}: $V_{1/2}$ = −19.5 ± 0.5 mV and z = 1.87 ± 0.05; 10 mM Ca^{2+}: $V_{1/2}$ = 6.8 ± 1.9 mV and z = 1.42 ± 0.06. (B) Ig traces recorded in the presence of 2 mM Ca^{2+} (control) and 10 mM Ca^{2+} at a test potential of +60 mV. Ig_{OFF} was measured at −110 mV. (C) Ig_{OFF} traces from B are shown at expanded time (initial 5 ms) and amplitude scales. (D) Gating currents of WT hERG1 channels measured during 300-ms pulses to +40 mV with a holding and return potential of −110 mV. Q_{OFF}-V relationships are shown in G. Extracellular concentrations of Ca^{2+} and Cd^{2+} are indicated to the left of the current traces. (E) Expanded view of initial Ig_{OFF} for the traces shown in D. (F) Currents recorded from an uninjected oocyte using the same pulse protocol as in D with the indicated concentrations of extracellular divalent cations. (G) Q_{OFF}-V relationship determined in a single oocyte in the presence of the indicated concentrations of extracellular Ca^{2+} and Cd^{2+}. For 2 mM Ca^{2+}: $Q_{OFF\text{-}max}$ = −8.0 nC, $V_{1/2}$ = −19.6 mV, and z = 2.2. For 10 mM Ca^{2+}: $Q_{OFF\text{-}max}$ = −12.0 nC, $V_{1/2}$ = +7.3 mV, and z = 1.6. For 10 mM Ca^{2+} + 0.1 mM Cd^{2+}: $Q_{OFF\text{-}max}$ = −9.3 nC, $V_{1/2}$ = +32 mV, and z = 1.1.

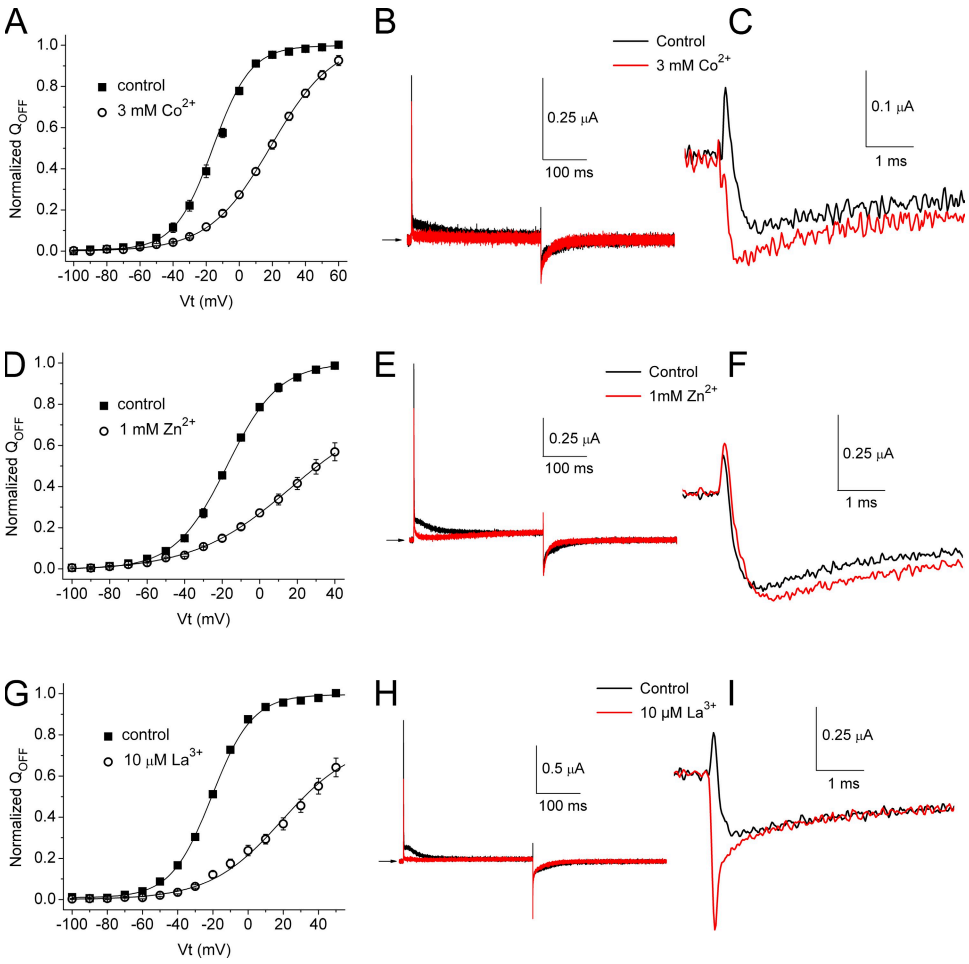

Figure 8. Co^{2+}, Zn^{2+}, and La^{3+} cause a positive shift in the voltage dependence of Q_{OFF}-V relationships for hERG1, but they do not induce a transient outward component in Ig_{OFF}. (A) Q_{OFF}-V relationships for hERG1 measured under control conditions ($[Ca^{2+}]_e$ = 2 mM) and after the addition of 3 mM Co^{2+} (n = 3). Control: $V_{1/2}$ = −15.9 ± 0.8 mV and z = 2.20 ± 0.08; Co^{2+}: $V_{1/2}$ = 19.1 ± 0.9 mV and z = 1.34 ± 0.02. (B) Ig traces recorded in the presence of 2 mM Ca^{2+} (control) and 3 mM Co^{2+} at a test potential of +60 mV. Ig_{OFF} was measured at −110 mV. (C) Ig_{OFF} traces from B are shown at expanded time (initial 5 ms) and amplitude scales. (D) Q_{OFF}-V relationships for hERG1 measured under control conditions ($[Ca^{2+}]_e$ = 2 mM) and after the addition of 1 mM Zn^{2+} (n = 3). Control: $V_{1/2}$ = −17.5 ± 0.3 mV and z = 1.82 ± 0.03; Zn^{2+}: $V_{1/2}$ = 16.4 ± 6.3 mV and z = 0.97 ± 0.06. (E) Ig traces recorded in the presence of 2 mM Ca^{2+} (control) and 1 mM Zn^{2+} at a test potential of +60 mV. Ig_{OFF} was measured at −110 mV. (F) Ig_{OFF} traces from E are shown at expanded time (initial 5 ms) and amplitude scales. (G) Q_{OFF}-V relationships for hERG1 measured under control conditions ($[Ca^{2+}]_e$ = 2 mM) and after the addition of 10 μM La^{3+} (n = 3). Control: $V_{1/2}$ = −20.6 ± 0.4 mV and z = 2.18 ± 0.06; La^{3+}: $V_{1/2}$ = 19.3 ± 3.9 mV and z = 1.23 ± 0.08. (H) Ig traces recorded in the presence of 2 mM Ca^{2+} (control) and 10 μM La^{3+} at a test potential of +60 mV. Ig_{OFF} was measured at −110 mV. (I) Ig_{OFF} traces from H are shown at expanded time (initial 5 ms) and amplitude scales.

current is attributed to movements of the VSD. The movements are thought to be associated with transitions between multiple closed states with little to no charge associated with transitions between a final closed state and the open state (C↔O). In contrast, previous models of hERG1 channel gating, including our own, assumed that significant charge displacement is associated with C↔O transitions and between open and inactivated states (O↔I) (Lu et al., 2001; Mazhari et al., 2001; Piper et al., 2003; Perry et al., 2007). However, as described below, the effects of a hERG1 agonist on channel gating suggest that C↔O transitions are not accompanied with a measurable component of charge.

RPR260243 ((3*R*,4*R*)-4-[3-(6-methoxy-quinolin-4-yl)-3-oxo-propyl]-1-[3-(2,3,5-trifluorophenyl)-prop-2-ynyl]-piperidine-3-carboxylic acid) is a recently described hERG1 channel activator that causes a marked slowing in the rate of deactivation. At 10 μM, RPR260243 slowed the rate of deactivation of ionic currents by at least 20-fold (Kang et al., 2005; Perry et al., 2007); however,

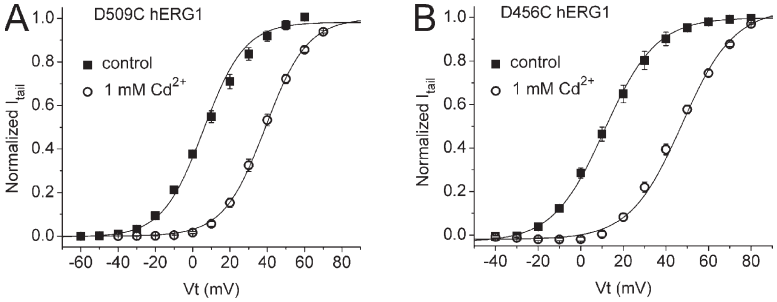

Figure 9. Extracellular Cd^{2+} induces positive shifts in the G-V relationships of D509C and D456C hERG1 channels. (A and B) G-V relationships for D509C hERG1 (A; n = 6) and D456C hERG1 (B; n = 5) channel currents in the absence (control) and presence of 1 mM extracellular Cd^{2+}.

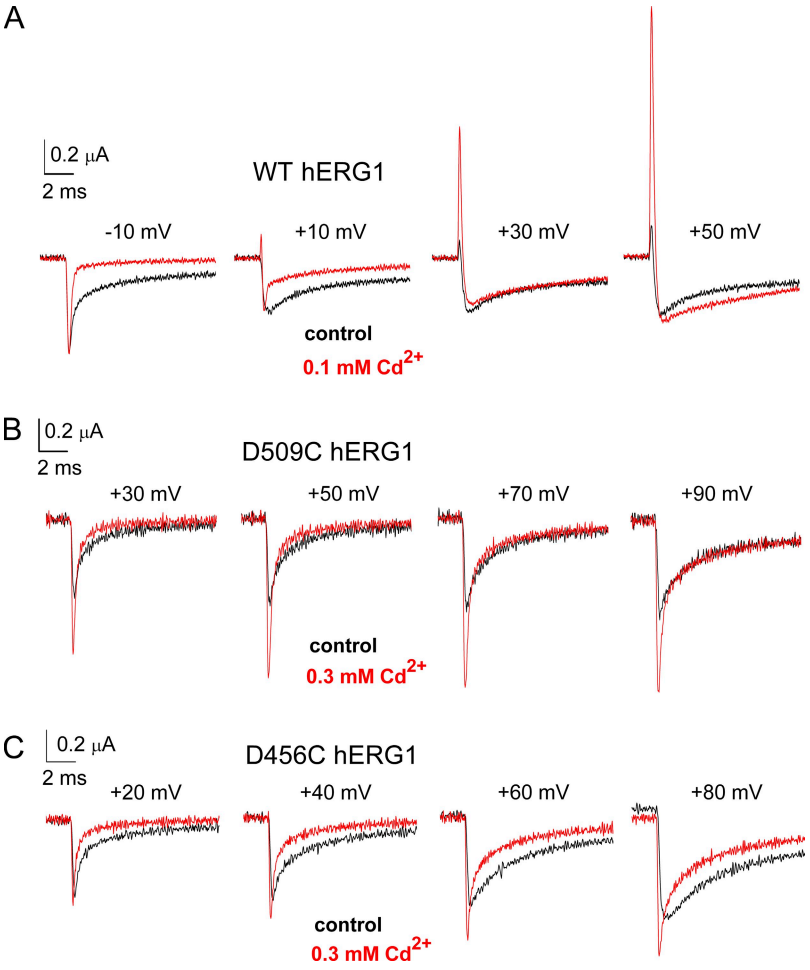

Figure 10. Cd^{2+} enhances $I_{Cd\text{-}out}$ of WT but not D509C or D456C hERG1 channels. (A) Traces for initial 10 ms of Ig_{OFF} of WT hERG1 channels elicited by return of membrane potential to −110 mV from the indicated V_t. (B and C) Traces for initial 10 ms of Ig_{OFF} of D509C (B) or D456C hERG1 (C) hERG1 channels elicited by return of membrane potential to −110 mV from the indicated V_t. Current traces for mutant channels are aligned below the traces for WT channels to facilitate comparisons based on measured shifts in the $V_{1/2}$ for activation of ionic currents. For all panels, black traces represent control currents, and red traces represent currents after treatment of an oocyte with 0.1 mM (WT channels) or 0.3 mM (mutant channels) $CdCl_2$.

as shown in Fig. 11 A, RPR260243 at 30 μM had no discernable effect on the kinetics or magnitude of Ig_{ON} or Ig_{OFF} at any potential examined. It also had no effect on the Q_{OFF}-V relationship (n = 5; Fig. 11 B). Thus, RPR260243 dissociates channel closure, as quantified by the rate of ionic current deactivation, from the movement of intramembrane gating charge. For this reason, we chose to develop a new Markov model that describes hERG1 gating currents as intramembrane charge displacement associated solely with transitions between closed states.

The standard Markov model (in the absence of Cd^{2+}) was developed to reconstruct gating currents measured with the standard voltage clamp protocol: 300-ms pulses to voltages ranging from −100 to +60 mV, applied from a holding potential of −110 mV and followed by

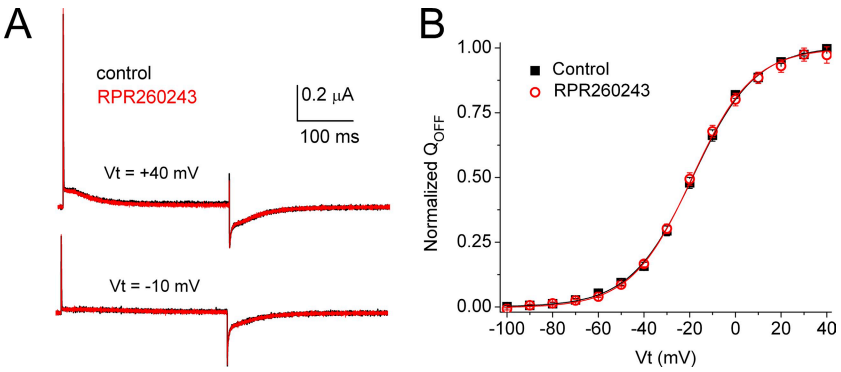

Figure 11. RPR260243 has no effect on hERG1 channel gating currents. (A) Gating currents for WT hERG1 channels measured at test potentials of −10 and +40 mV before (black traces) or 25 min after exposure of an oocyte to 30 μM RPR260243 (red traces). For these experiments, the currents were filtered at 5 kHz and digitized at 20 kHz. (B) Average Q_{OFF}-V relationships determined under control conditions and after the treatment of the same oocytes with 30 μM RPR260243 for 20–25 min (n = 5). Q_{OFF} was normalized to the peak of the control value for each oocyte. Data were fitted with a Boltzmann function (smooth curves). In control conditions, $V_{1/2}$ = −18.6 ± 0.5 mV and z = 1.84 ± 0.01. In the presence of RPR260243, $V_{1/2}$ = −19.0 ± 0.5 mV and z = 1.88 ± 0.01.

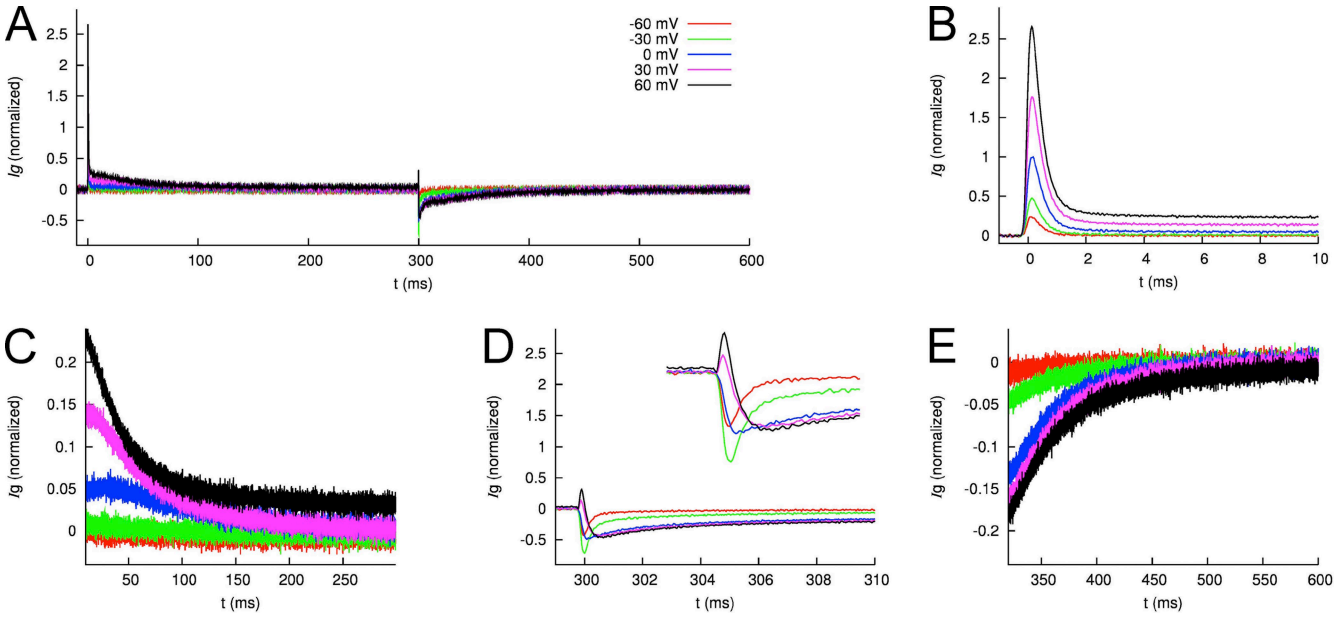

Figure 12. Averaged and normalized *Ig* of WT hERG1 channels measured using p/−8 leak and capacitance current subtraction. (A) *Ig* in response to test voltages V_t of −60, −30, …+60 mV during 0–300 ms. The membrane voltage is clamped to −110 mV otherwise. (B and C) Ig_{ON} at 0–10 ms and 10–300 ms, respectively. (D and E) Ig_{OFF} at 300–310 ms and 310–600 ms, respectively.

repolarization to −110 mV for 300 ms. Parameters of the standard model were determined by a numerical fitting procedure to features extracted from averaged (n = 12) and normalized gating currents for WT hERG1 channels (Fig. 12). A schematic of the standard Markov model for gating of WT hERG1 channels is shown in Fig. 13, where states S_0 to S_{14} (A) define VSD movements, and the states C_0, C_1, O, and I (B) reflect activation and

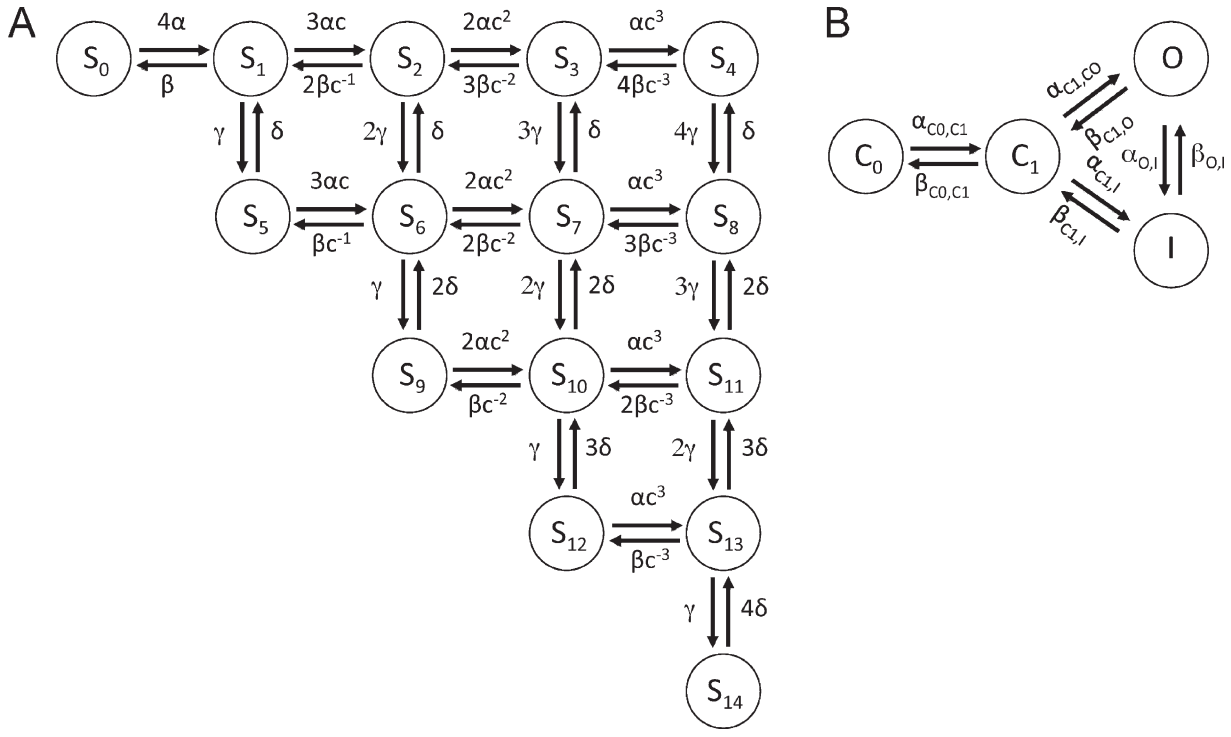

Figure 13. Schematics of Markov model for gating and ionic currents of WT hERG1 channels. The model consists of two components, one for voltage sensing with the states S_0 to S_{14} (A) and the other for activation and inactivation with the states C_0, C_1, O, and I (B). The coupling between the components is via the rate coefficient $\alpha_{C0,C1}$, which is a function of the states S_4, S_8, S_{11}, S_{13}, and S_{14} in the component for voltage sensing.

inactivation of the pore domain. Transitions between all states in the model satisfy the condition of microscopic reversibility. Features and fit errors associated with parameterization of the VSD model (Fig. 13 A) are listed in Table S1. Fig. 14 shows a comparison between these features extracted from the measured and simulated data. The total gating charge for the model was 5.1 e_0.

Gating currents simulated with the standard model are presented in Fig. 15. The simulations showed instantaneous peak outward current in response to test voltages followed by a plateau current (Fig. 15 B) that decayed slowly (Fig. 15 C). Repolarization to −110 mV caused an instantaneous inward current followed by a plateau (Fig. 15 D) and slowly decaying current (Fig. 15 E). The standard model explains the instantaneous Ig_{ON} peak by gating current associated with the fast transition between S_0 and S_1 (Fig. 15 F). The model suggests that the plateau component of Ig_{ON} is a mixture of decreasing and increasing currents. Simulated plateau Ig_{ON} is primarily composed of decreasing gating currents associated with S_1–S_5, S_2–S_6, S_3–S_7, and S_4–S_8 transitions and increasing currents of S_6–S_9, S_7–S_{10}, S_8–S_{11}, S_{10}–S_{12}, S_{11}–S_{13}, and S_{13}–S_{14} transitions (Fig. 15 G).

Several variants of the standard model were studied to evaluate cooperativity and parameterization of the activation/inactivation component. Allowing for cooperativity of the fast transitions in the numerical fitting procedure had only minor effects on the fit error and yielded cooperativity factors close to 1, suggesting no cooperativity of these transitions. Previously published models (Lu et al., 2001; Perry et al., 2007) were tested for parameterization of the activation/inactivation component of the standard model (Fig. 13 B). The inclusion of these models into the standard model increased the fit error, in particular, errors associated with features of Ig_{OFF}.

The Cd^{2+} model was parameterized using features extracted from averaged ($n = 10$) and normalized data measured for WT hERG1 channels in the presence of 100 µM Cd^{2+} (Fig. 16). A schematic of the Markov model for the *Ig* of hERG1 channels in the presence of extracellular Cd^{2+} is presented in Fig. 17. States S_0 to S_{14} describe configurations of the hERG1 tetramer with two Cd^{2+} ions bound at sites in the resting configuration of the VSDs. States S_{15} to S_{24}, and S_{25} to S_{30}, are color coded and depict hERG1 channel configurations having one and two Cd^{2+} ions moved inwardly from

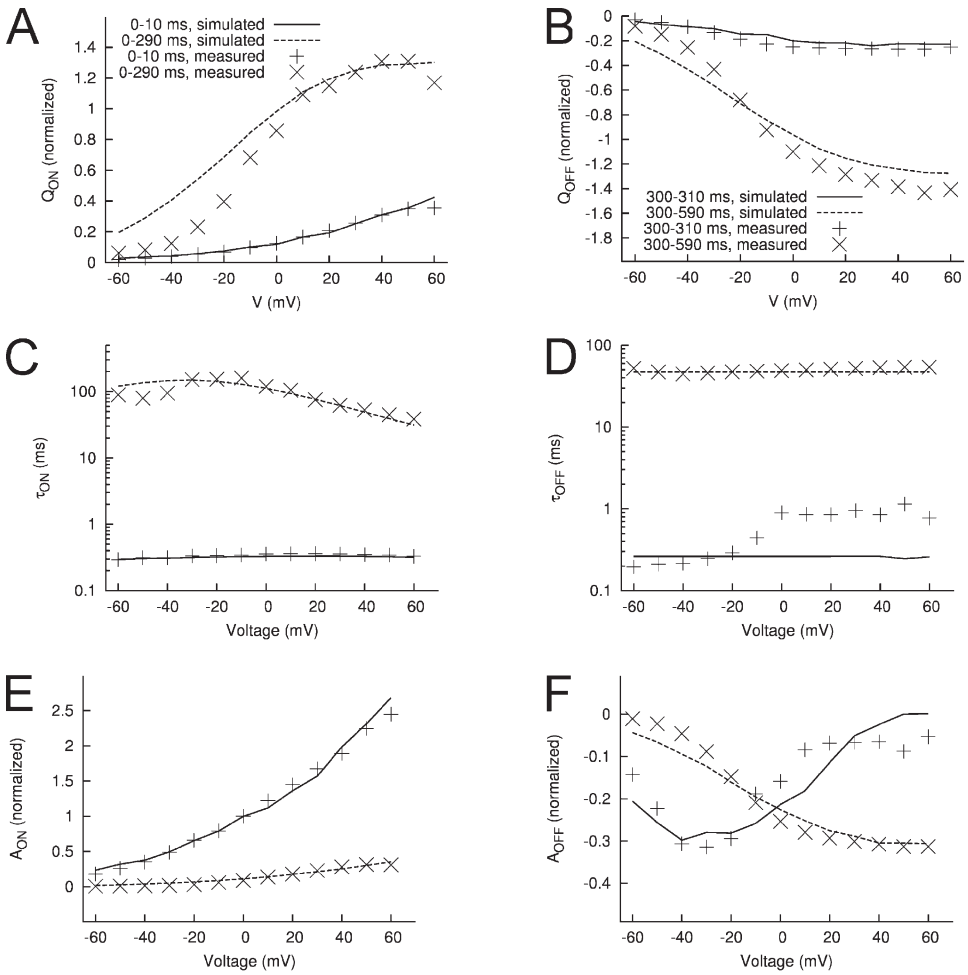

Figure 14. Features of measured and modeled I_g. Q-V_t relationships for Ig_{ON} (A) and Ig_{OFF} (B). Time constants–V_t relationships for Ig_{ON} (C) and Ig_{OFF} (D). Relationship of exponential fit coefficients to V_t for Ig_{ON} (E) and Ig_{OFF} (F).

their original VSD binding sites, respectively. Transitions between all states in the Cd^{2+} model satisfy the condition of microscopic reversibility. Features and fit errors for the standard and Cd^{2+} models are listed in Table S1. Tables S2 and S3 list the initial parameters and rate constants for transitions between channel states for both models. In Fig. 18, we compare features extracted from measured data to features from simulated data. Gating currents simulated with the Cd^{2+} model are presented in Fig. 19. The model reconstructed the decreased peak and plateau of Ig_{ON} (Fig. 19 B), attenuated slow decay of Ig_{ON} (Fig. 19 C) and outward current $I_{Cd\text{-}out}$ (Fig. 19 D), and accelerated slow decay of Ig_{OFF} for positive voltage steps. The model explains these phenomena by a current I_{Cd} associated with Cd^{2+} displacement from one binding site to another. I_{Cd} is opposite to components of Ig related to transitions between closed states (Fig. 19 F). The contribution of gating (VSD movement) and Cd^{2+} currents to the outward component of Ig_{OFF} is further detailed in Fig. 19 G. $I_{Cd\text{-}out}$ is dominated by transitions between states with one and two Cd^{2+} ions moved outward relative to their positions occupied when the VSDs are in their activated position.

DISCUSSION

Extracellular Cd^{2+} alters hERG1 channel gating

Extracellular application of Cd^{2+} caused a concentration-dependent shift of the Q_{OFF}-V relationship to more positive potentials, similar to our previously reported shift in the G-V relationship for hERG1 ionic currents (Fernandez et al., 2005). The shifted Q_{OFF}-V relationship was accompanied by an alteration in the kinetics of Ig_{ON} and Ig_{OFF}. These kinetic changes included both a slowing and reduction in the slow component of Ig_{ON}, and for Ig_{OFF}, a slowing of the initial slow component and an acceleration of the late slow component, thus creating a crossover with the control Ig_{OFF}. In addition, Cd^{2+} induced the appearance of a large transient outward current component of Ig_{OFF} ("$I_{Cd\text{-}out}$"). We propose that all of these effects of Cd^{2+} are mediated by

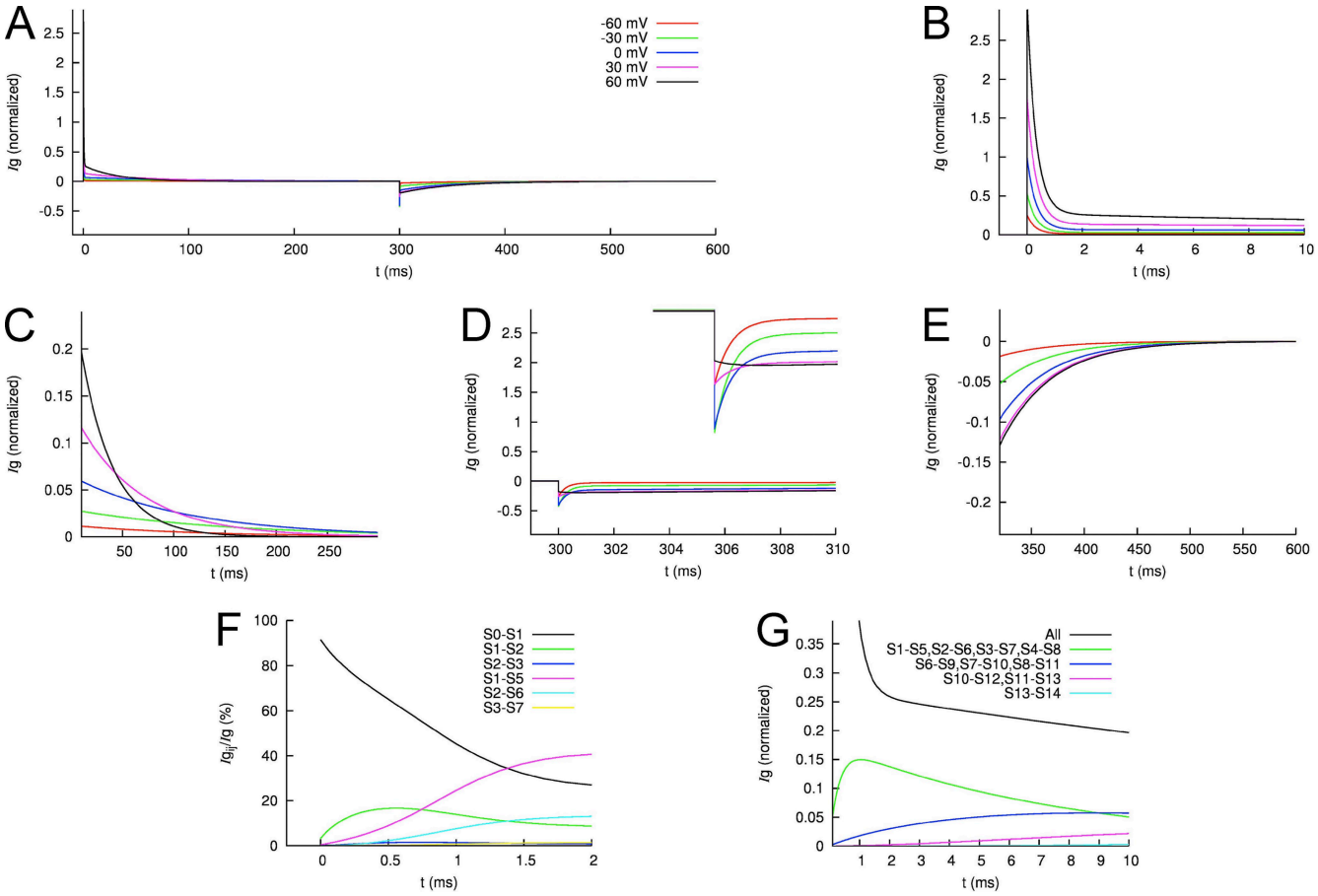

Figure 15. Modeled *Ig* of WT hERG1 channels. (A) *Ig* in response to the voltage-clamping protocol used in Fig. 12. (B and C) Ig_{ON} at 0–10 ms and 10–300 ms, respectively. (D and E) Ig_{OFF} at 300–310 ms and 310–600 ms, respectively. (F) The initial phase (0–1 ms) of Ig_{ON} is primarily carried by the fast transition between S_0 and S_1. (G) The slow decay of Ig_{ON} between 2 and 10 ms is caused by a mixture of increasing and decreasing gating currents associated with the slow transitions in the gating model.

its interaction with an extracellular, accessible coordination site formed by acidic residues in the S2 (D456 and D460) and S3 (D509) segments of each hERG1 subunit. We previously found that charge neutralization of any one of these acidic residues reduced the Cd^{2+}-induced shift in the G-V relationship, and that combined mutation of all three residues nearly eliminated the effects of Cd^{2+} on hERG1 channel gating (Fernandez et al., 2005). In addition to the kinetic effects described above, prolonged incubation of oocytes with Cd^{2+} was associated with a reduction in total Q_{OFF}, an effect that may be associated with a slow accumulation of cytoplasmic Cd^{2+}.

Origin of $I_{Cd\text{-}out}$

Extracellular Cd^{2+} induced a brief outward current ($I_{Cd\text{-}out}$) that coincided with repolarization from test potentials positive to 0 mV to a negative holding potential and preceded the inward component of Ig_{OFF}. The appearance of $I_{Cd\text{-}out}$ associated with membrane repolarization was unexpected and counterintuitive, as normally a hyperpolarizing pulse produces only an inwardly directed charge displacement. However, the magnitude of $I_{Cd\text{-}out}$, quantified as either peak amplitude or by its integral, was increased by 3 to 300 µM Cd^{2+} in a concentration-dependent manner.

Even in the absence of extracellular Cd^{2+}, a small outward component of Ig_{OFF} was observed that coincided with repolarization from positive test potentials in oocytes expressing hERG1 (Fig. 3 C). The charge associated with the outward current under control conditions amounted to only 0.3% of the total Q_{OFF}. The origin of this tiny outward current is uncertain, but it is related to overexpression of hERG1 channels because it was not observed in uninjected oocytes. The current could be an experimental artifact related to the use of the on-line p/−8 subtraction procedure if channels were not fully closed at the holding potential used for the linear leak/capacitance subtraction pulses (−110 mV in our experiments), as assumed previously for other Kv channels (Stühmer et al., 1991). However, Sigworth (1994) recorded a similar outward current that preceded inward Ig_{OFF} in oocytes expressing Shaker K^+ channels and suggested that it might represent a decrease in capacitance due to a change in polarizability (e.g., reorientation of side chains of polar amino acids) associated with a change in channel states. In Shaker channels, the integral of this small current for a step from +40 to −100 mV was only 0.3% of the total Q_{OFF} (Sigworth, 1994), the same as we recorded for hERG1 channels with a similar step in voltage (Fig. 5 D). One possible explanation of $I_{Cd\text{-}out}$ is that it represents an extreme (>10-fold) increase in polarization of the channel, but this seems unlikely given the absence of the current component in D456C or D509C channels treated with Cd^{2+} or in WT hERG1 channels exposed to other divalent cations.

An outward current component of Ig_{OFF} was not observed under control conditions for mutant D509C or D456C hERG1 channels. Moreover, $I_{Cd\text{-}out}$ was not induced by Cd^{2+} concentrations that caused significant changes in the kinetics of inward Ig_{OFF} and significant rightward shifts in the voltage dependence of channel activation. One interpretation of this finding could be that inward displacement of S2 and S3 (and thus, D509 and D456) precedes S4 movement to produce the

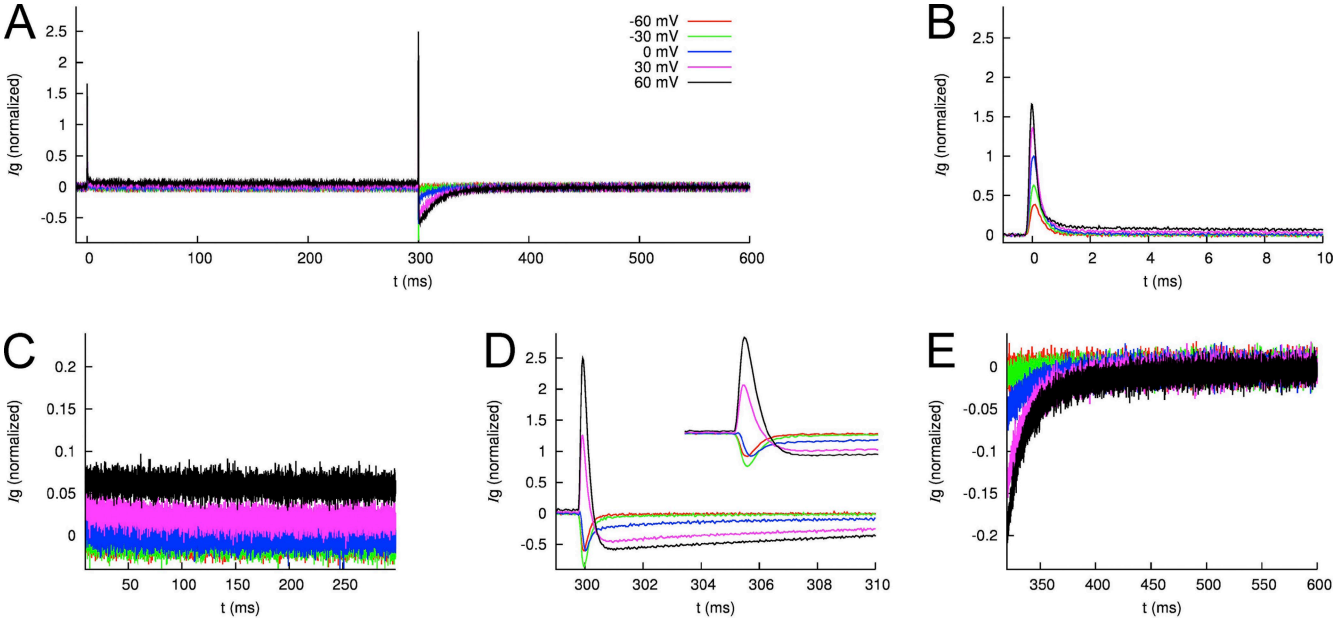

Figure 16. Averaged and normalized *Ig* of WT hERG1 channels measured in the presence of extracellular Cd^{2+}. (A) *Ig* measured with test voltages V_t of −60, −30,…+60 mV. The membrane voltage is −110 mV otherwise. (B and C) Ig_{ON} at 0–10 ms and 10–300 ms, respectively. (D and E) Ig_{OFF} at 300–310 ms and 310–600 ms, respectively.

outward component of Ig_{OFF}, and that in the presence of Cd^{2+}, this movement is accentuated in WT channels and absent in mutant channels where these acidic residues are neutralized. However, available evidence suggests that S2 and S3 segments of Kv channels either do not move during gating or that the S3b and S4 segments move together (and not in opposite directions) across the membrane as a rigid "paddle" structure (Jiang et al., 2003). The large intramembrane displacement of S3b/S4 proposed by the paddle model has been challenged (Ahern and Horn, 2005; Tombola et al., 2006), and a recent luminescence resonance energy transfer study estimated that although the S4 segment of Shaker moves ~10 Å during gating, the S3 segment moves only ~2 Å and in the opposite direction (Posson and Selvin, 2008). Neutralization of the two acidic residues in the S3 of Shaker also failed to impact the gating charge in Shaker channels (Gonzalez et al., 2005). These and other studies suggest that the S3 segment has only a minor or no role in the net intramembrane charge displacement associated with Shaker channel gating. In contrast, the acidic residue in S2 of Shaker is estimated by luminescence resonance energy transfer to move ~4 Å outward during gating (Posson and Selvin, 2008) and thus contributes to the total gating charge, as suggested previously (Seoh et al., 1996). In summary, based on studies of other Kv channels, an S4-independent, accentuated inward displacement of S2 and/or S3 segments in response to repolarization is very unlikely to produce the outward component of Ig_{OFF} either in the absence or presence of extracellular Cd^{2+}. Instead, we propose that $I_{Cd\text{-}out}$ represents an outward ionic current conducted by Cd^{2+}, as it is displaced in an extracellular direction from its coordination site between the S2 and S3 segments as described below.

The voltage-dependent activation gating of ion channels is associated with sequential ion pair formation between basic residues in the mobile S4 segment and specific acidic residues in the fixed S2 segments. In the closed state of Kv channels (Silverman et al., 2003) and NaChBac channels (DeCaen et al., 2008, 2009), a specific basic residue ("R1") located in the outer region of S4 charge pairs with an acidic residue in S2 ("D1"). Membrane depolarization causes outward movement of S4 and sequential ion pair formation between D1 and different Arg residues. In the fully activated state, "R3"

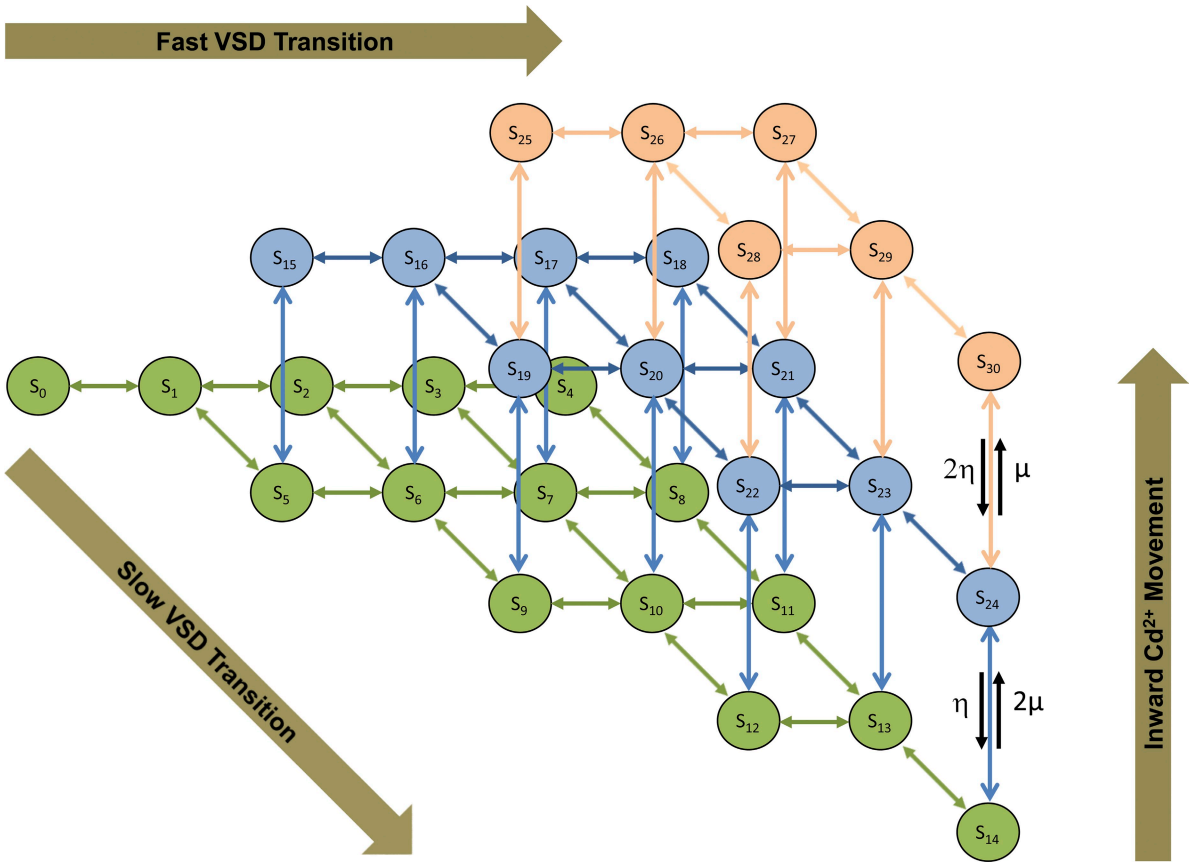

Figure 17. Schematics of Markov model for *Ig* of WT hERG1 channels in the presence of extracellular Cd^{2+}. The model extends the description of *Ig* in Fig. 13 A with states and transitions describing the movement of Cd^{2+}. States S_0 to S_{14} (green) describe hERG1 configurations with Cd^{2+} bound to a site in the VSD. States S_{15} to S_{24} (blue), and S_{25} to S_{30} (brown), are associated with hERG1 configurations having one and two Cd^{2+} ions moved in the VSD, respectively.

and/or "R4" of S4 forms the final electrostatic interaction with D1. hERG1 subunits contain two additional acidic residues, D460 in S2 and D509 in S3, that are not present in the more well-studied Shaker, Kv1.2, KvAP, and NaChBac channels. As noted previously, both of these acidic residues are important components of the coordination site for Cd^{2+} (Fernandez et al., 2005), and based on double-mutant cycle analysis, both are energetically coupled to R531 (R3) during hERG1 channel gating (Piper et al., 2008). The importance of D456 and D509 in hERG1 gating is exemplified by the finding that neutralization of either residue causes large positive shifts in the voltage dependence of channel activation (Liu et al., 2003; Fernandez et al., 2005; Lin and Papazian, 2007; Piper et al., 2008). Thus, it is likely that in addition to the well-characterized electrostatic interactions between R1 and D1 in Kv channels, D2 (D456) and D3 (D509) of hERG1 subunits also interact with basic residues in the S4 during channel gating.

The details of hERG1 channel gating with regard to sequential ion pairing between charged residues in S4 and S2/S3 have not yet been systematically elucidated. Nonetheless, we propose a simple gating model to explain the origin of $I_{Cd\text{-}out}$. An outward displacement of Cd^{2+} (opposite to electrical driving force) could be driven by an appropriate change in the highly localized electrostatic energy associated with the coordination of Cd^{2+}. It is conceivable that only a subtle movement of S4 is required to alter the structural basis of the Cd^{2+} coordination site; e.g., by favoring charge pairing between an Asp in S2 or S3 with an Arg in S4 instead of with Cd^{2+}. A net outward current ($I_{Cd\text{-}out}$) could be produced if the initial voltage-induced change in S4 displacement produced a small inward gating current relative to a much larger outward current associated with a change in the coordination site for Cd^{2+}. The model, illustrated in Fig. 20, shows the orientation of S2–S4 of the VSD for a single hERG1 subunit and highlights the key charged residues in these segments. K1 (equivalent to R1 in other channels) plus R2–R4 represent the basic residues in S4, and D1–D3 represent Asp residues located near the extracellular ends of S2 and S3 as indicated.

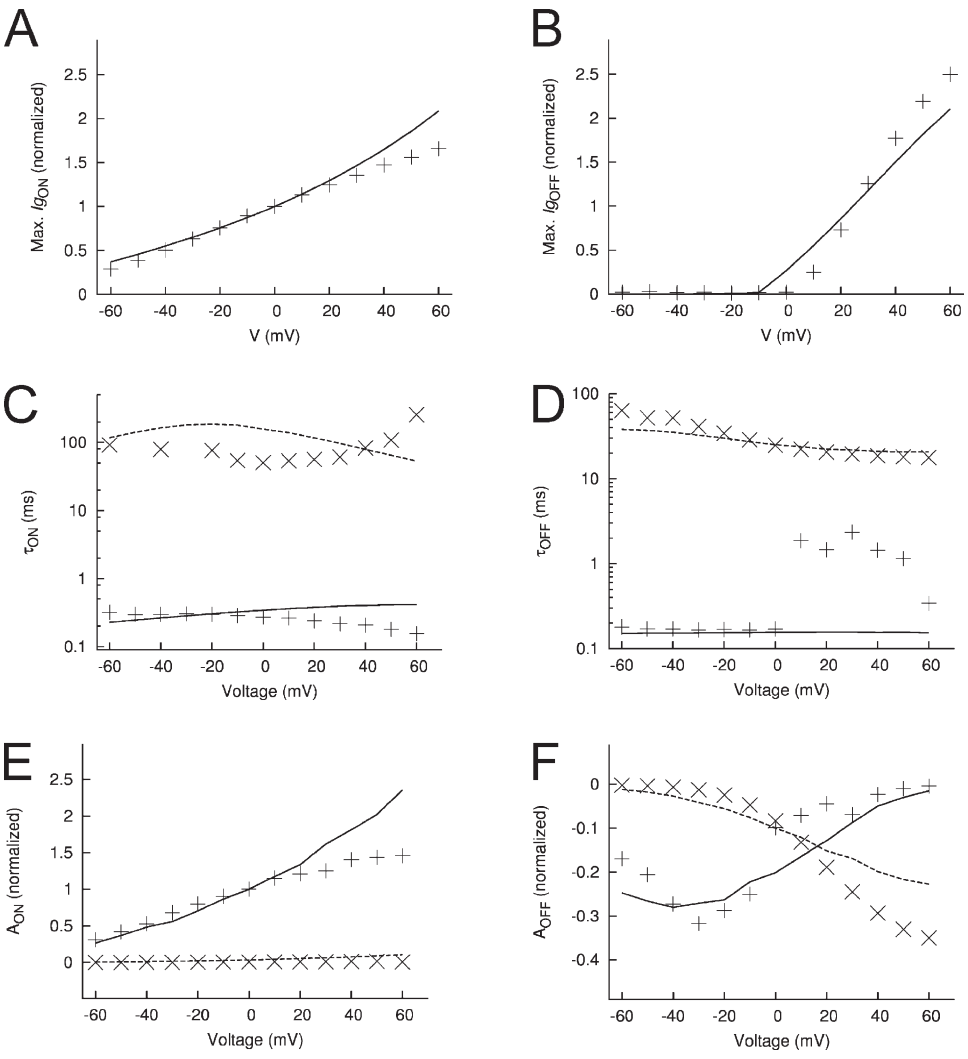

Figure 18. Features of measured and modeled *Ig* in the presence of extracellular Cd^{2+}. (A) Maximal Ig_{ON}-V_t relationship. (B) Maximal Ig_{OFF}-V_t relationship. Time constants–V_t relationships for Ig_{ON} (C) and Ig_{OFF} (D). Relationship of exponential fit coefficients to V_t for Ig_{ON} (E) and Ig_{OFF} (F).

At depolarized potentials when channels are in the open state, R531 (R3) forms an ion pair with D456 (D1), and Cd^{2+} interacts with its "depolarized" coordination site. Repolarization induces inward movement of S4 and displacement of Cd^{2+}, first by R528 (R2) and then by K525 (K1). Because $I_{Cd\text{-}out}$ is an outward current, we propose that Cd^{2+} is displaced in an outward direction compared with its "depolarized" coordination site. For example, the depolarized coordination site could be formed by D456, D460, and D509 (D1, D2, and D3), whereas the "repolarized" coordination site for Cd^{2+} might be formed primarily by the outermost Asp residues, D456 and D509.

Disruption of the normal electrostatic interactions between S4 and S2/S3 by Cd^{2+} or other divalent cations causes a positive shift in the voltage dependence of hERG1 channel activation. Neutralization of D456 or D509 by mutation to the uncharged Cys would obviously prevent their electrostatic interaction with S4. However, Cys can coordinate Cd^{2+} ions as effectively as does Asp (Rulísek and Vondrásek, 1998) and thus, it was not unexpected that Cys substitutions only modestly attenuated the Cd^{2+}-induced positive shift in the voltage dependence of activation. However, $I_{Cd\text{-}out}$ was not observed for either mutant channel, perhaps because Cd^{2+} is situated in a slightly different molecular space when coordinated by a Cys instead of an Asp and is not displaced by movement of S4. Alternatively, inward S4 movement might displace Cd^{2+} in a lateral or inward direction relative to the transmembrane electric field when its coordination site is formed in part by a Cys rather than an Asp residue.

The other polyvalent metal cations examined in this study, Ca^{2+}, Co^{2+}, Zn^{2+}, and La^{3+}, did not induce an outward current similar to $I_{Cd\text{-}out}$ at concentrations that caused positive shifts in the Q_{OFF}-V or G-V relationships approximately equivalent to that produced by 0.1 mM Cd^{2+}.

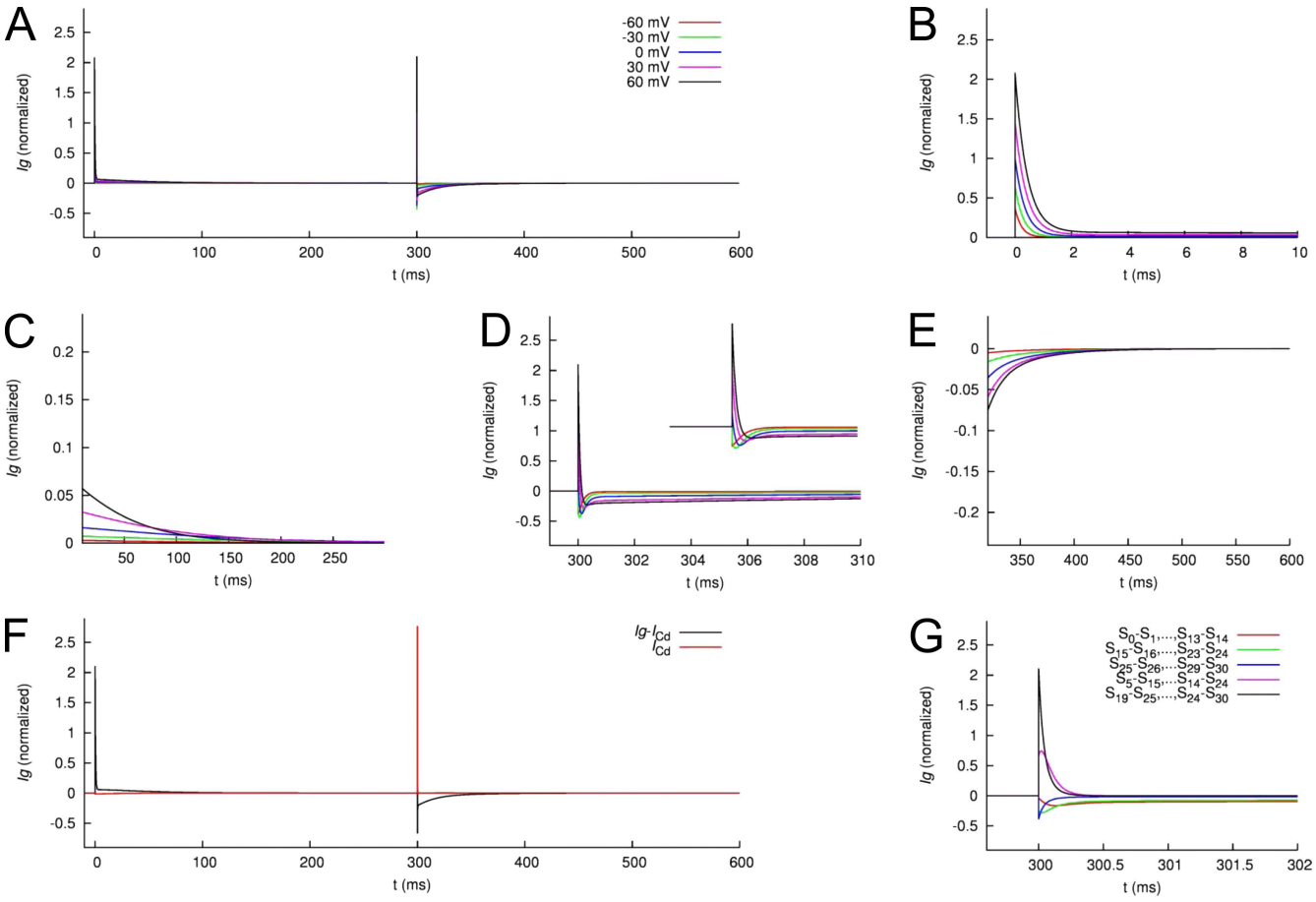

Figure 19. Modeled *Ig* of WT hERG1 channels in the presence of extracellular Cd^{2+}. (A) *Ig* in response to the voltage-clamping protocol used in Fig. 12. (B and C) Ig_{ON} at 0–10 ms and 10–300 ms, respectively. (D and E) Ig_{OFF} at 300–310 ms and 310–600 ms, respectively. (F) Gating current (*Ig*) caused by movement of VSD and current conducted by Cd^{2+} (I_{Cd}) for a 300-ms voltage step to +60 mV, followed by a return to the holding potential of −110 mV. The sum of these two currents produces the gating currents simulated to occur in the presence of Cd^{2+}. (G) Currents underlying the initial 2 ms of Ig_{OFF} (300–302 ms). Major contributors to initial Ig_{OFF} are Cd^{2+}currents (I_{Cd}) related to transitions between S_{19}–S_{25} and S_{24}–S_{30} (black) and between S_5–S_{15} and S_{14}–S_{24} (pink). Currents related to VSD movement (red, green, and blue) have a small contribution to initial Ig_{OFF} but dominate after decay of I_{Cd}.

This could again be explained if movement of S4 did not displace these cations or if their displacement produced an undetectable current (e.g., masked by inward Ig_{OFF}).

Modulation of hERG1 channel gating by extracellular Ca^{2+}

The Q_{OFF}-V relationship for hERG1 was shifted by +26 mV and $Q_{OFF\text{-}max}$ was increased by 44% when $[Ca^{2+}]_e$ was elevated from 2 to 10 mM. The subsequent addition of 100 µM Cd^{2+} caused a further positive shift in the voltage dependence of gating and returned $Q_{OFF\text{-}max}$ to a value similar to that recorded in the presence of 2 mM Ca^{2+}. It is unclear how elevated $[Ca^{2+}]_e$ caused the increase in $Q_{OFF\text{-}max}$, but it was not simply caused by an accelerated return of charge (leading to an increased integration over the 300-ms sampling period at −110 mV) because the same acceleration caused by Cd^{2+}, Co^{2+}, or Zn^{2+} was not accompanied by an increase in $Q_{OFF\text{-}max}$. Recruitment of channels to the cell membrane could increase $Q_{OFF\text{-}max}$, but forward trafficking of channels is expected to be far slower than the rapid onset of the gating changes induced by elevated Ca^{2+}. Moreover, an increase in $[Ca^{2+}]_e$ from 2.5 to 10 mM actually diminishes the magnitude of ionic current, an effect attributed to external pore block (Ho et al., 1998).

The finding that Cd^{2+} returned $Q_{OFF\text{-}max}$ to a value similar to that recorded in the presence of 2 mM Ca^{2+} suggests that extracellular Cd^{2+} and Ca^{2+} compete for an overlapping binding site. We previously reported that the effects of Ca^{2+} on hERG1 ionic currents were most attenuated by neutralization of D456 or a combination of D456 and D509. In contrast, Mg^{2+} binding to hERG1 was largely determined by D456, with a lesser contribution from D460 and D509 (Fernandez et al., 2005; Lin and Papazian, 2007). This finding supports the idea that the S2/S3 binding site for divalent cations overlaps, but that they are not identical. Moreover, the shift in the Q_{OFF}-V relationship by Ca^{2+} plus Cd^{2+} was less than additive, inconsistent with these cations binding to distinct sites on the channel.

RPR260243 dissociates gating currents from ionic currents of hERG1

RPR260243 is a hERG1 channel activator. Site-directed mutagenesis was used to localize its binding site to specific residues in the S5 and S6 segments and nearby S4–S5 linker (Perry et al., 2007). The location of this binding site helps to explain its ability to markedly slow the rate of deactivation of hERG1 ionic current (Kang et al., 2005). Unexpectedly, RPR260243 had no detectable effect on the kinetics, magnitude, or voltage dependence of hERG1 gating currents. The same remarkable dissociation between effects on ionic and gating currents was recently reported for FPL 64176 on L-type $Ca_V1.2$ channels. To explain this dissociation, it was proposed that when bound by FPL 64176, $Ca_V1.2$ channels conduct Ca^{2+} in the inactivated state without having any affect on the rates of VSD movement (McDonough et al., 2005). We propose that RPR260243 (a) has no effect on the rates of transitions between closed states of the hERG1 channel and thus produces no change in the kinetics or magnitude of gating currents, and (b) slows the transition of the open to the closed state of the pore domain. Thus, similar to the action of FPL 64176 on $Ca_V1.2$, RPR260243 dissociates gating charge displacement (VSD movement) from the opening and closing of the activation gate formed by the S6 bundle crossing.

Gating models

A novel feature of our Markov model for hERG1 channel gating is the decoupling of VSD movements ($S_0 \leftrightarrow S_1,\ldots,S_{13} \leftrightarrow S_{14}$ transitions) from the opening, closing, and inactivation of the pore domain ($C_0 \leftrightarrow C_1 \leftrightarrow O \leftrightarrow I$ transitions). Implicit in this model is that the transitions

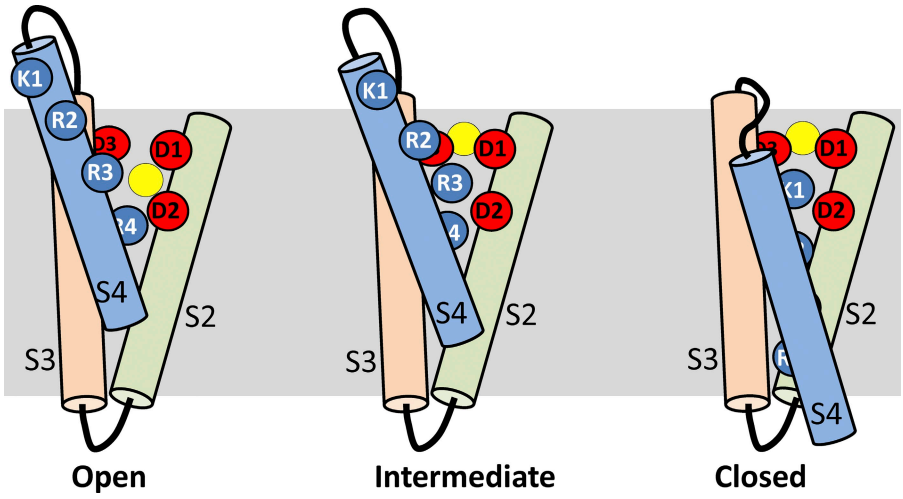

Figure 20. Schematic showing state-dependent positions of Cd^{2+} and key charged residues in S2–S4 segments of the VSD of a single hERG1 channel subunit. According to this model, Cd^{2+} is displaced in an outward direction by basic residues in the S4 segment as it moves inward in response to membrane repolarization. (Left) VSD at depolarized potentials and Cd^{2+} in its "depolarized" coordination site. (Right) VSD at a negative transmembrane potential when all channels are closed and Cd^{2+} located in a position defined as the "repolarized" coordination site. (Middle) A putative intermediate state of the channel. K1, K525; R2, R528; R3, R531; R4, R534; D1, D456; D2, D460; D3, D509. The yellow circle represents a Cd^{2+} ion.

between states S_0 to S_{14} describe the vast majority of charge displacement. Some previous Markov models of hERG1 included a significant amount of total charge displacement associated with the gating between the final closed state and the open and inactivated state (Lu et al., 2001; Mazhari et al., 2001; Piper et al., 2003; Perry et al., 2007). In addition, as summarized in Table I, our model assumes no cooperativity for the VSD displacement, similar to the original Shaker model (Zagotta et al., 1994), but unlike a later Shaker model (Schoppa and Sigworth, 1998) or our previous hERG model (Piper et al., 2003) that used a cooperativity factor of 1.3–1.5, respectively. Finally, the total gating charge estimated for the model was 5.1 e_0. This is 2.7-fold less than that estimated from experimental data for Shaker K^+ channels (~13.6 e_0) (Schoppa et al., 1992; Aggarwal and MacKinnon, 1996). The total gating charge per hERG1 channel (z_{total}) has not been determined. However, the *z* value obtained from the fitting of Q-V relationships for hERG1 is ~2 (Fig. 2 D) versus ~7 for Shaker channels (Olcese et al., 1997), a 3.5-fold difference.

The Cd^{2+} model assumes that two out of four Cd^{2+} binding sites in the VSD hERG1 channels are occupied, and that rearrangement of the VSD facilitates displacement of Cd^{2+} from a site to another position in close proximity. During activation, slow VSD transitions precede the inward Cd^{2+} movement, which is oppositely directed to the electrical field. The structural basis of the Cd^{2+} binding site was not investigated in this study, but based on our previous work (Fernandez et al., 2005), extracellular Cd^{2+} binds to a coordination site formed by three specific acidic residues in S2/S3; inward or outward displacement of Cd^{2+} from this site in response to channel activation or deactivation, respectively, could generate I_{Cd}. The charge displacement associated with I_{Cd} was estimated in the model to be 0.2 e_0 for each Cd^{2+} displaced. Assuming that on average half the Cd^{2+} binding sites were occupied per channel, the charge associated with $I_{Cd\text{-}out}$ would be equivalent to ~8% of the magnitude of the total charge modeled for the $S_0 \leftrightarrow S_{14}$ transitions (5.1 e_0) for a single channel. The maximum value of the ratio $Q_{Cd\text{-}out}/Q_{OFFtotal}$ expressed as a percent was ~6% (Fig. 5 E). This measured value is necessarily an underestimate because $Q_{Cd\text{-}out}$ was defined as the integral of $I_{Cd\text{-}out}$ and thus was decreased by the overlap of the initial rapid component of inward Ig_{OFF}. Assuming that half of the Cd^{2+} coordination sites (two of four sites occupied for a total Cd^{2+} charge of +4) are occupied at 100–300 μM Cd^{2+} (EC_{50} = 171 μM), it can be estimated that the $I_{Cd\text{-}out}$ measured after pulsing to a test potential of +60 mV could be produced by two Cd^{2+} ions traversing ~8% ($[5.1e_0 \times 0.06]/4 = 0.077$) of the transmembrane electric field.

The standard and Cd^{2+} Markov hERG1 gating models have several limitations. First, the models do not describe ionic currents through hERG1 channels. Parameterization of the activation/inactivation component (Fig. 13 B) based on previous models of hERG1 channel currents was not possible due to their large gating currents associated with C↔O and O↔I. The finding indicates that redesign of this model component will be necessary. Such a redesign might also help with solving discrepancies between experimental and modeling data for the time constant of the fast component of Ig_{OFF} at voltages >0 mV (Figs. 14 D and 18 D). Second, the presented simulations do not account for system functions of the measurement devices and signal processing. In particular, applying a low-pass filter at 10 kHz as in the measurements to the modeled *Ig* would reduce the differences in the responses of *Ig* to voltage steps. Third, the Cd^{2+} model was designed for reproducing measured data for $[Cd^{2+}]_e$ of 100 μM that we assumed to cause two bound Cd^{2+} per hERG1 channel. The model does not reconstruct $[Cd^{2+}]_e$-dependent effects. Although not a focus of the presented study, the model could be extended for this purpose, e.g., by integration with models for one, three, and four bound Cd^{2+} per hERG1 channel. Fourth, the fitting process did not yield unique solutions for parameters of the Cd^{2+} model, in particular, the Cd^{2+} movement parameters (μ_0, z_μ, η_0, z_η, and z_{Cd}).

TABLE I

Rate constant and charge parameters of Kv channel gating models

Model	Transitions	α_0 [s^{-1}]	z_α	β_0 [s^{-1}]	z_β	c
Zagotta et al. 1994 (Shaker channel)	R_1–R_2	1,120	0.25	373	1.6	1
	R_2–A	2,800	0.32	21.2	1.1	1
Schoppa and Sigworth 1994 (Shaker channel)	S_0–S_1	1,650	0.47	450	0.52	1.3
	S_1–S_2	4,900	0.08	960	0.52	1
	S_2–S_3	7,920	0.08	1,560	0.52	1
Piper et al. 2003 (hERG1 channel)	S_0–S_1	1,000	0.2	1,500	0.04	1
	S_1–S_2	150	0.15	280	0.05	1.5
Standard model (hERG1 channel)	fast (e.g., S_0–S_1)	296	0.43	2,683	0.076	1
	slow (e.g., S_4–S_8)	73	0.21	1.9	0.56	1
Cd^{2+} model (hERG1 channel)	fast (e.g., S_0–S_1)	563	0.27	2,329	0.23	1
	slow (e.g., S_4–S_8)	20.9	0.30	5.7	0.68	1

Other parameter sets yielded similar fit errors, perhaps because the transitions between the different Cd^{2+}-bound levels are not exponential processes.

Summary

Cd^{2+} shifted the voltage dependence of the Q-V relationship for hERG1 channels in accordance with the positive shift of the G-V relationship for ionic currents. Cd^{2+} also induced the appearance of a transient outward current, $I_{Cd\text{-}out}$, upon repolarization from test potentials above 0 mV. Collectively, our present and previous (Fernandez et al., 2005) findings suggest that: (a) at depolarized potentials, extracellular Cd^{2+} binds to a "depolarized" coordination site formed by acidic residues located in the S2/S3 segments of each subunit; (b) with membrane repolarization, Cd^{2+} is displaced to accommodate sequential electrostatic interactions between Arg residues in S4 and acidic residues in S2 and S3 that are required for inward movement of S4; (c) outward displacement of Cd^{2+} to its "repolarized" coordination site produces $I_{Cd\text{-}out}$; and (d) inward movement of S4 does not require similar displacement of Ca^{2+}, Co^{2+}, Zn^{2+}, or La^{3+} (or Cd^{2+} when bound to D456C or D509C hERG1 channels), or if they are displaced, these cations move in a lateral or inward direction relative to the cell membrane and thus do not produce an outward current.

New Markov models of hERG1 channel gating were formulated. Gating currents are described as noncooperative transitions between multiple closed states of the channel with no charge displacement associated with transitions to or from the open or inactivated states. The finding that RPR260243 markedly slows deactivation of ionic currents without having any effect of gating currents provided experimental support for this model.

This work was supported by National Institutes of Health/National Heart, Lung and Blood Institute grants HL65299 and HL55236.

Edward N. Pugh Jr. served as editor.

Submitted: 8 April 2010
Accepted: 6 July 2010

REFERENCES

Aggarwal, S.K., and R. MacKinnon. 1996. Contribution of the S4 segment to gating charge in the *Shaker* K^+ channel. *Neuron.* 16:1169–1177. doi:10.1016/S0896-6273(00)80143-9

Ahern, C.A., and R. Horn. 2005. Focused electric field across the voltage sensor of potassium channels. *Neuron.* 48:25–29. doi:10.1016/j.neuron.2005.08.020

Anumonwo, J.M., J. Horta, M. Delmar, S.M. Taffet, and J. Jalife. 1999. Proton and zinc effects on HERG currents. *Biophys. J.* 77:282–298. doi:10.1016/S0006-3495(99)76889-X

Armstrong, C.M., and F. Bezanilla. 1977. Inactivation of the sodium channel. II. Gating current experiments. *J. Gen. Physiol.* 70:567–590. doi:10.1085/jgp.70.5.567

Cherny, V.V., and T.E. DeCoursey. 1999. pH-dependent inhibition of voltage-gated H^+ currents in rat alveolar epithelial cells by Zn^{2+} and other divalent cations. *J. Gen. Physiol.* 114:819–838. doi:10.1085/jgp.114.6.819

Curran, M.E., I. Splawski, K.W. Timothy, G.M. Vincent, E.D. Green, and M.T. Keating. 1995. A molecular basis for cardiac arrhythmia: *HERG* mutations cause long QT syndrome. *Cell.* 80:795–803. doi:10.1016/0092-8674(95)90358-5

DeCaen, P.G., V. Yarov-Yarovoy, Y. Zhao, T. Scheuer, and W.A. Catterall. 2008. Disulfide locking a sodium channel voltage sensor reveals ion pair formation during activation. *Proc. Natl. Acad. Sci. USA.* 105:15142–15147. doi:10.1073/pnas.0806486105

DeCaen, P.G., V. Yarov-Yarovoy, E.M. Sharp, T. Scheuer, and W.A. Catterall. 2009. Sequential formation of ion pairs during activation of a sodium channel voltage sensor. *Proc. Natl. Acad. Sci. USA.* 106:22498–22503. doi:10.1073/pnas.0912307106

Fernandez, D., A. Ghanta, K.I. Kinard, and M.C. Sanguinetti. 2005. Molecular mapping of a site for Cd^{2+}-induced modification of human ether-à-go-go-related gene (hERG) channel activation. *J. Physiol.* 567:737–755. doi:10.1113/jphysiol.2005.089094

Follmer, C.H., N.J. Lodge, C.A. Cullinan, and T.J. Colatsky. 1992. Modulation of the delayed rectifier, I_K, by cadmium in cat ventricular myocytes. *Am. J. Physiol.* 262:C75–C83.

Gonzalez, C., F.J. Morera, E. Rosenmann, O. Alvarez, and R. Latorre. 2005. S3b amino acid residues do not shuttle across the bilayer in voltage-dependent Shaker K^+ channels. *Proc. Natl. Acad. Sci. USA.* 102:5020–5025. doi:10.1073/pnas.0501051102

Ho, W.-K., I. Kim, C.O. Lee, and Y.E. Earm. 1998. Voltage-dependent blockade of HERG channels expressed in *Xenopus* oocytes by external Ca^{2+} and Mg^{2+}. *J. Physiol.* 507:631–638. doi:10.1111/j.1469-7793.1998.631bs.x

Jiang, Y., V. Ruta, J. Chen, A. Lee, and R. MacKinnon. 2003. The principle of gating charge movement in a voltage-dependent K^+ channel. *Nature.* 423:42–48. doi:10.1038/nature01581

Johnson, J.P. Jr., J.R. Balser, and P.B. Bennett. 1999a. Enhancement of HERG K(+) currents by $Cd^{(2+)}$ destabilization of the inactivated state. *Biophys. J.* 77:2534–2541. doi:10.1016/S0006-3495(99)77088-8

Johnson, J.P. Jr., F.M. Mullins, and P.B. Bennett. 1999b. Human ether-à-go-go–related gene K^+ channel gating probed with extracellular ca^{2+}. Evidence for two distinct voltage sensors. *J. Gen. Physiol.* 113:565–580. doi:10.1085/jgp.113.4.565

Johnson, J.P. Jr., J.R. Balser, and P.B. Bennett. 2001. A novel extracellular calcium sensing mechanism in voltage-gated potassium ion channels. *J. Neurosci.* 21:4143–4153.

Kang, J., X.L. Chen, H. Wang, J. Ji, H. Cheng, J. Incardona, W. Reynolds, F. Viviani, M. Tabart, and D. Rampe. 2005. Discovery of a small molecule activator of the human ether-a-go-go-related gene (HERG) cardiac K^+ channel. *Mol. Pharmacol.* 67:827–836. doi:10.1124/mol.104.006577

Keating, M.T., and M.C. Sanguinetti. 2001. Molecular and cellular mechanisms of cardiac arrhythmias. *Cell.* 104:569–580. doi:10.1016/S0092-8674(01)00243-4

Lin, M.C., and D.M. Papazian. 2007. Differences between ion binding to eag and HERG voltage sensors contribute to differential regulation of activation and deactivation gating. *Channels (Austin).* 1:429–437.

Liu, J., M. Zhang, M. Jiang, and G.N. Tseng. 2003. Negative charges in the transmembrane domains of the HERG K channel are involved in the activation- and deactivation-gating processes. *J. Gen. Physiol.* 121:599–614. doi:10.1085/jgp.200308788

Lu, Y., M.P. Mahaut-Smith, A. Varghese, C.L. Huang, P.R. Kemp, and J.I. Vandenberg. 2001. Effects of premature stimulation on HERG $K(^+)$ channels. *J. Physiol.* 537:843–851. doi:10.1113/jphysiol.2001.012690

Mazhari, R., J.L. Greenstein, R.L. Winslow, E. Marbán, and H.B. Nuss. 2001. Molecular interactions between two long-QT syndrome gene products, HERG and KCNE2, rationalized by in vitro and in silico analysis. *Circ. Res.* 89:33–38. doi:10.1161/hh1301.093633

McDonough, S.I., Y. Mori, and B.P. Bean. 2005. FPL 64176 modification of $Ca_V1.2$ L-type calcium channels: dissociation of effects on ionic current and gating current. *Biophys. J.* 88:211–223. doi:10.1529/biophysj.104.051714

Olcese, R., R. Latorre, L. Toro, F. Bezanilla, and E. Stefani. 1997. Correlation between charge movement and ionic current during slow inactivation in Shaker K^+ channels. *J. Gen. Physiol.* 110:579–589. doi:10.1085/jgp.110.5.579

Perry, M., F.B. Sachse, and M.C. Sanguinetti. 2007. Structural basis of action for a human ether-a-go-go-related gene 1 potassium channel activator. *Proc. Natl. Acad. Sci. USA.* 104:13827–13832. doi:10.1073/pnas.0703934104

Piper, D.R., A. Varghese, M.C. Sanguinetti, and M. Tristani-Firouzi. 2003. Gating currents associated with intramembrane charge displacement in HERG potassium channels. *Proc. Natl. Acad. Sci. USA.* 100:10534–10539. doi:10.1073/pnas.1832721100

Piper, D.R., J. Rupp, F.B. Sachse, M.C. Sanguinetti, and M. Tristani-Firouzi. 2008. Cooperative interactions between R531 and acidic residues in the voltage sensing module of hERG1 channels. *Cell. Physiol. Biochem.* 21:37–46. doi:10.1159/000113745

Posson, D.J., and P.R. Selvin. 2008. Extent of voltage sensor movement during gating of shaker K^+ channels. *Neuron.* 59:98–109. doi:10.1016/j.neuron.2008.05.006

Press, W.H., S.A. Teukolsky, W.T. Vetterling, and B.P. Flannery. 1992. Numerical Recipes in C. 2nd ed. Cambridge University Press, Cambridge. 994 pp.

Rulísek, L., and J. Vondrásek. 1998. Coordination geometries of selected transition metal ions (Co^{2+}, Ni^{2+}, Cu^{2+}, Zn^{2+}, Cd^{2+}, and Hg^{2+}) in metalloproteins. *J. Inorg. Biochem.* 71:115–127. doi:10.1016/S0162-0134(98)10042-9

Sanchez-Chapula, J.A., and M.C. Sanguinetti. 2000. Altered gating of HERG potassium channels by cobalt and lanthanum. *Pflugers Arch.* 440:264–274.

Sanguinetti, M.C. 2010. HERG1 channelopathies. *Pflugers Arch.* 460:265–276. doi:10.1007/s00424-009-0758-8

Sanguinetti, M.C., and M. Tristani-Firouzi. 2006. hERG potassium channels and cardiac arrhythmia. *Nature.* 440:463–469. doi:10.1038/nature04710

Sanguinetti, M.C., C. Jiang, M.E. Curran, and M.T. Keating. 1995. A mechanistic link between an inherited and an acquired cardiac arrhythmia: *HERG* encodes the I_{Kr} potassium channel. *Cell.* 81:299–307. doi:10.1016/0092-8674(95)90340-2

Schoppa, N.E., and F.J. Sigworth. 1998. Activation of Shaker potassium channels. III. An activation gating model for wild-type and V2 mutant channels. *J. Gen. Physiol.* 111:313–342. doi:10.1085/jgp.111.2.313

Schoppa, N.E., K. McCormack, M.A. Tanouye, and F.J. Sigworth. 1992. The size of gating charge in wild-type and mutant *Shaker* potassium channels. *Science.* 255:1712–1715. doi:10.1126/science.1553560

Seoh, S.-A., D. Sigg, D.M. Papazian, and F. Bezanilla. 1996. Voltage-sensing residues in the S2 and S4 segments of the *Shaker* K^+ channel. *Neuron.* 16:1159–1167. doi:10.1016/S0896-6273(00)80142-7

Sigworth, F.J. 1994. Voltage gating of ion channels. *Q. Rev. Biophys.* 27:1–40. doi:10.1017/S0033583500002894

Silverman, W.R., B. Roux, and D.M. Papazian. 2003. Structural basis of two-stage voltage-dependent activation in K^+ channels. *Proc. Natl. Acad. Sci. USA.* 100:2935–2940. doi:10.1073/pnas.0636603100

Stefani, E., and F. Bezanilla. 1998. Cut-open oocyte voltage-clamp technique. *In* Methods in Enzymology. P.N. Conn, editor. Academic Press, San Diego. 300–318.

Stühmer, W. 1992. Electrophysiological recording from *Xenopus* oocytes. *Methods Enzymol.* 207:319–339. doi:10.1016/0076-6879(92)07021-F

Stühmer, W., F. Conti, M. Stocker, O. Pongs, and S.H. Heinemann. 1991. Gating currents of inactivating and non-inactivating potassium channels expressed in *Xenopus* oocytes. *Pflugers Arch.* 418:423–429. doi:10.1007/BF00550881

Tombola, F., M.M. Pathak, and E.Y. Isacoff. 2006. How does voltage open an ion channel? *Annu. Rev. Cell Dev. Biol.* 22:23–52.

Trudeau, M.C., J.W. Warmke, B. Ganetzky, and G.A. Robertson. 1995. HERG, a human inward rectifier in the voltage-gated potassium channel family. *Science.* 269:92–95. doi:10.1126/science.7604285

Warmke, J.W., and B. Ganetzky. 1994. A family of potassium channel genes related to *eag* in *Drosophila* and mammals. *Proc. Natl. Acad. Sci. USA.* 91:3438–3442. doi:10.1073/pnas.91.8.3438

Zagotta, W.N., T. Hoshi, J. Dittman, and R.W. Aldrich. 1994. Shaker potassium channel gating. II: transitions in the activation pathway. *J. Gen. Physiol.* 103:279–319. doi:10.1085/jgp.103.2.279